Master Thesis
TVVR 22/5008

Sediment Transport and Erosion in Viskan River, South Sweden

Siyuan Wang

Division of Water Resources Engineering
Department of Building and Environmental Technology
Lund University

Sediment Transport and Erosion in Viskan River, South Sweden

By:
Siyuan Wang

Master Thesis

Division of Water Resources Engineering
Department of Building & Environmental Technology
Lund University
Box 118
221 00 Lund, Sweden

Water Resources Engineering
TVVR-22/5008
ISSN 1101-9824

Lund 2022
www.tvrl.lth.se

Master Thesis
Division of Water Resources Engineering
Department of Building & Environmental Technology
Lund University

Swedish title:	Sedimenttransport och erosion i Viskan
English title:	Sediment Transport and Erosion in Viskan River, South Sweden
Author(s):	Siyuan Wang
Supervisor:	Prof. Magnus Larson Eng. Fainaz Inamdeen
Examiner:	Dr. Rolf Larsson
Language	English
Year:	2022
Keywords:	HEC-RAS, cross section, erosion, sediment transport, deposition

Acknowledgements

First of all, from the bottom of my heart, I am taking this opportunity to convey my sincere gratitude to my Supervisor Professor Magnus Larson of the Department of Water Resources Engineering, Lund University, for his counsel, encouragement, and worthwhile amazing supervision in the course of the study.

Secondly, special appreciation goes to my co-supervisor Fainaz Inamdeen also from Department of Water Resources Engineering, Lund University for his guidance, assistance and providing all the needed information for the study.

Thirdly, many thanks go to Adnan Drobic from Swedish Geotechnical Institute (SGI) for his valuable assistance in guiding me the field trip along Viskan and providing valuable information.

Furthermore, my sincere gratitude to SWECO and Vattenfall in providing bathymetry data and calibration data which is the basis of this study.

Lastly, I'm profoundly grateful to my family for their financial and moral support throughout the time of my study, without them, I would not have made it this far.

Abstract

This master thesis study presents the results of sediment transport analysis along Viskan, located in south Sweden. The main processes cover building a hydrodynamic model, studying parameters that define sediment transport, modelling sediment transport within the river, mapping out erosive stretches and comparing to observed eroded locations, and finally comparison of different transport functions how they influence the results. The study section has a total distance of 33.78 km. In HEC-RAS, the one-dimensional model was employed. To build the model on the already provided Digital Elevation Model, the HEC-RAS Mapper was used. Steady flow and sediment transport simulations were then done to obtain the hydrodynamics and sediment transport of the river respectively. After sediment transport simulations, 5 most eroded cross sections: cross section (XS) 2374, XS 38919, XS 45988, XS 49945 and XS 88725 are used for possible causes analysis. Then the observed erosion compared with simulation results was taken and all the cross sections are shown reasonable results from HEC-RAS. Furthermore, the comparison of the Meyer-Peter and Müller transport function, the Laursen (Copeland) transport function, the Engelund-Hansen transport functions and the Wilcock-Crowe transport function were analyzed. Results show the Engelund-Hansen transport functions are more sensitive for deposition and the Meyer-Peter and Müller transport function is the most balanced function with the gentlest changes.

Keywords:
HEC-RAS, cross section, erosion, sediment transport, deposition

Table of contents

List of Figures

List of Tables

1 Introduction

The theory of sediment transport is the focus of very intense research which is going on all over the world. The main source of sediment in natural streams are erosion by overland flow, stream-channel erosion, bank cutting and supply from small erosion channels formed in unconsolidated soil (Engelund and Hansen, 1967). Moreover, the upland erosion by water can be classified into sheet erosion and rill erosion. When the rainfall starts the surface-erosion will start by the raindrop hitting the ground and detaching soil particles by splash (Julien, 2018).

Sediment transport is the movement of solid particles including sand, gravel, clay etc., typically due to the shear stress caused by water flow and sediment has reached the threshold of motion (Soulsby, 1997). Most rivers run through areas consisting of loose material that may be transported by the flowing water, causing erosion or accumulation of material at specific locations along the river. For instance, there might be soil erosion, local scour around structures and beach erosion if erosion occurs. As for accumulation there might be reservoir sedimentation, infilling of harbors, navigation channels and water intakes. A wide range of engineering problems are related to sediment transport including bank erosion, sedimentation in reservoirs, and general and local bed scour. The erosion rate depends on the flow and sediment properties and the hydraulic characteristics of the river (Soulsby, 1997). Furthermore, sediment derived from eroded land can be a major pollutant or a carried of polluting chemicals such as nutrients, pesticides, and contaminants like heavy metals and complex organic components. These pollutants can be transported dissolved or adsorbed to complex colloids (Brandt, 2017).

However, erosion and sediment transport in rivers have not been considered a serious environmental problem in Sweden except locally on agricultural land and when vegetation has been removed due to construction work (Brandt, 2017). Moreover, the field measurements are typically limited in space and time. There are some problems associated with sediment transport including erosion, deposition and reduction in bank stability have been noticed in the river Viskan. In order to analyze the sediment transport and its impact on the morphological evolution within Viskan modelling is typically needed since field measurements are lacking.

1.1 Background

The Viskan River is the northernmost of the four large rivers that flow out into the sea along the coastline of Halland. Some areas along the river are heavily populated and developed, including the city of Borås. Moreover, there are several hydropower plants in the river with lakes acting as storages which are delaying the river runoff (Modigh el al, 2012).

Along numerous stretches of the river erosion have been observed, primarily of the banks but most likely also the bed. Since the river bank material is fine in many places, having been deposited during the most recent ice age when the water level was higher (Modigh el al, 2012). Slides are common contributing to the sediment transport in the river and the erosion of the banks. Therefore, it is interested to understand and quantify the sediment transport and its impact on the morphological evolution, particularly regarding the erosion and where it occurs.

The Swedish Geotechnical Institute (SGI) is developing an index to determine whether erosion is likely to occur in a river based on easily available, schematic information to be analyzed in a GIS environment. The investigation proposed in the present study will assist in validating the methodology to determine the erosion index.

1.2 Objectives

The overall aim of this study is to determine the sediment transport in the Viskan and its impact on river morphology, with a particular focus on erosion stretches. The comprehensive evaluation of the erosion is based on available data and mathematical modelling for river stability analysis along the Viskan. Due to the size of the river catchment, the impact of the lakes, and the characteristics of the adjacent areas to the river, the works will emphasize parts of the river, rather than the whole river, where erosion is widespread.

The sub-objectives dealt with are as follows:

i. Build hydrodynamic model and study parameters that define sediment transport
ii. Model sediment transport within the river
iii. Assessing the implications for erosion
iv. Comparison different transport functions

1.3 Procedures

In order to attain the objectives, an extensive review of literature was conducted centering on sediment transport in rivers, flow modeling, river morphology. The literature review covered discussions on physical characteristics of the Viskan. Moreover, a literature review associated with theory of the sediment transport in rivers focus on erosive conditions was performed. Finally, a literature review was carried out concerning the hydraulic modelling approaches in HEC-RAS to understand how the modelling is conducted including the steady flow, sediment transport and erosion.

Data for river bathymetry came from SWECO and the river flows came from SMHI. The grain size distribution information was limited therefore this study combined the information from County Administrative Board of Västra Götaland and SGU. The gathered data was used for analysis, modelling and simulation in HEC-RAS. In HEC-RAS, firstly, simulated the steady flow condition to calculated velocities and shear stress and calibration with bathymetry. Then quasi-unsteady flow was considered in the modelling to apply for the sediment transport simulation.

Through simulations, hydraulic parameters and quantity of sediment transport along river were established. Moreover, the most erosive river locations were observed by HEC-RAS modelling. Then a comparison of observed erosion from field trip with the results from HEC-RAS was researched. Finally, the different transport functions are used in HEC-RAS to research how these functions influence the model.

1.4 Report Content

The major content of the report starts from Chapter 2 where the climatology and hydrology, river hydraulics, geomorphology and sediment transport, and river bank erosion and scour are discussed in detail. The report then proceeds to describe all theory behind river sediment transport including basic processes, mechanisms in sediment transport, how sediment is classified, types of loads and slope failure and bank stability in Chapter 3. In Chapter 4, the model theory on HEC-RAS is elucidated. The report does not end there but goes further to Chapter 5 where data used, and their sources are discussed. Aspects covered in Chapter 5 are a description of the bathymetry of the river, flow data, stage data, temperature, sediment data. The report further goes to Chapter 6 where model

simulations results are presented and also explained specifically concerning sensitivity analysis, steady flow, sediment transport within HEC-RAS. The report then dives into Chapter 7 where discussion of results as interpreted, and conclusions drawn are presented. Chapter 8 discusses the limitations faced during this study and also presents recommendations. Finally, the report ends with a list of references considered in the study and figures that could not be included in the main report are included in the appendices.

2 Viskan river

2.1 General

Viskan has a catchment area of approximately 2202 km^2 and extends over four municipalities and two counties which are Halland and Västra Götaland. Viskan river is starting in Lake Tolken in Ulricehamn municipality and ends after passing Mark and Borås in Klosterfjorden in Kattegatt, Varbergs municipality along a 142-km length. The largest tributaries are Häggån, Slottsån, Surtan, Lillån, Hornån and Skuttran. The total area is covered with 58% forest land, 15% agricultural land, 6% lake and 3% urban area (Modigh el al., 2012). The average annual discharge from the river is 43.2 m^3/s and the maximum yearly flow around 180 m^3/s. For the current study, a 33.78 km river reach from the coastal outlet and upstream was considered. Figure 1 below shows the location of Viskan river in south Sweden.

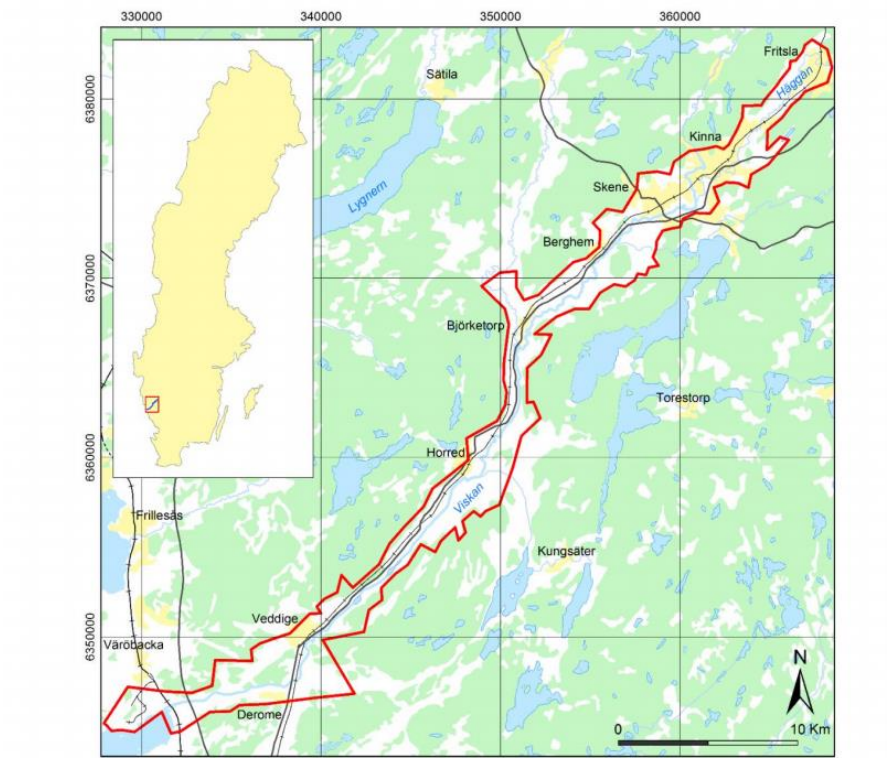

Figure 1. Overview map of the updated and described area in the Viskan and Häggån valleys (Engdahl and Pile, 2019)

According to SMHI, the main catchment is divided into 30 sub-catchments based on the main river and its tributaries. Since the studied river stretch is the downstream 33.78 km, there are only four catchments with a total area of about 80.5 km^2 adding water to the river, as shown in Figure 2.

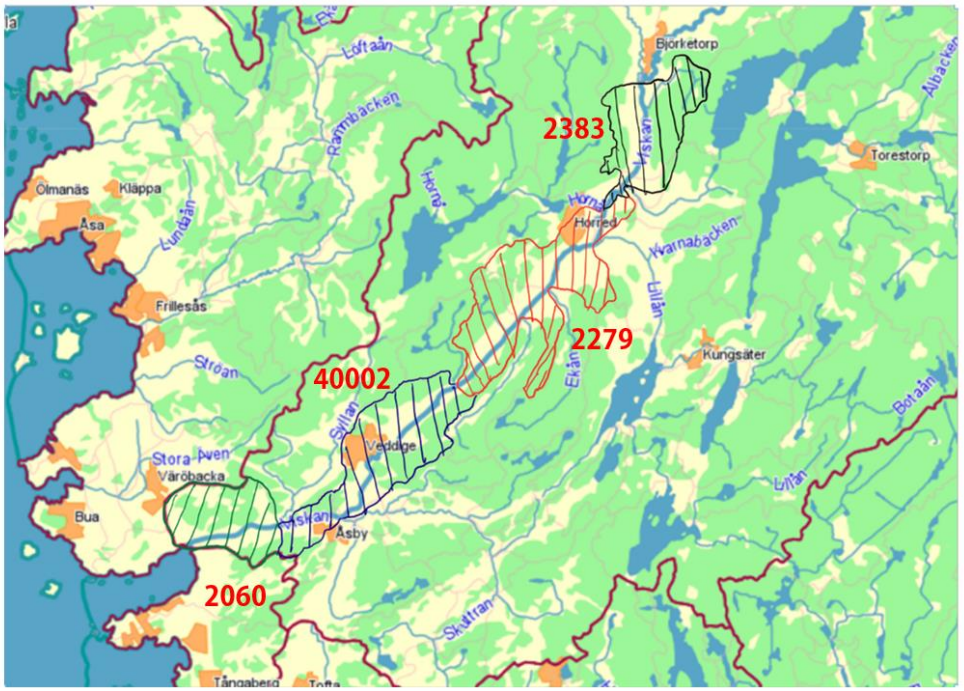

Figure 2. The sub catchments of Viskan basin aligned to the study area (Vattenwebb.smhi.se, 2022)

According to SGU (Geological Survey of Sweden), the bedrocks of the catchments are lightly eroded clay and silt dominate in Viskan's valley from the coast up to Kinna. Here are ravine landscapes with high natural values, often linked to deciduous forests and pastures. Further up and the boundaries of the catchment, the soil layers are dominated by moraine.

2.2 Climatology and Hydrology

Viskan is an elongated catchment area with a limited lake surface, which implies that the watercourse reacts relatively quickly to precipitation. This means that the high-water flows are often strong, but the flow returns to a much lower water flow are relatively quickly. High flows rarely last more than a

couple of days (Modigh el al., 2012). Due to various climatic conditions through the years, the annual average river flow may change dramatically between the years shown as Figure 3. More detailed daily river flow is shown in Chapter 5 Figure 35. Furthermore, according to the SMHI the average water temperature is 9.3°C.

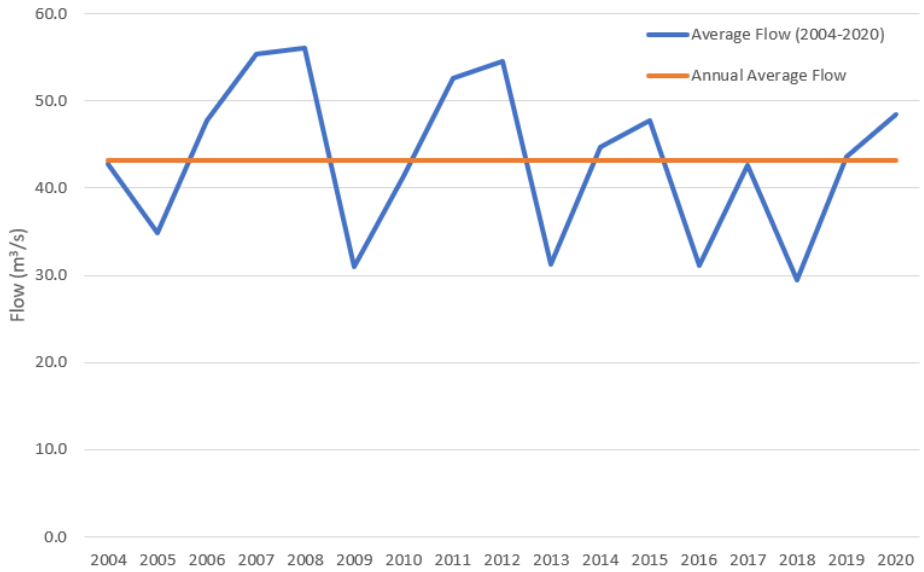

Figure 3. The annual average river flow for years 2004-2020

The highest water flows occur between November and February. The average water flow in January is approximately 71 m^3/s, while the corresponding value for June is 11 m^3/s at Kullagård in the lower part of Viskan (Modigh el al, 2012). Figure 4 below shows Viskan's monthly average water flow at Kullagård.

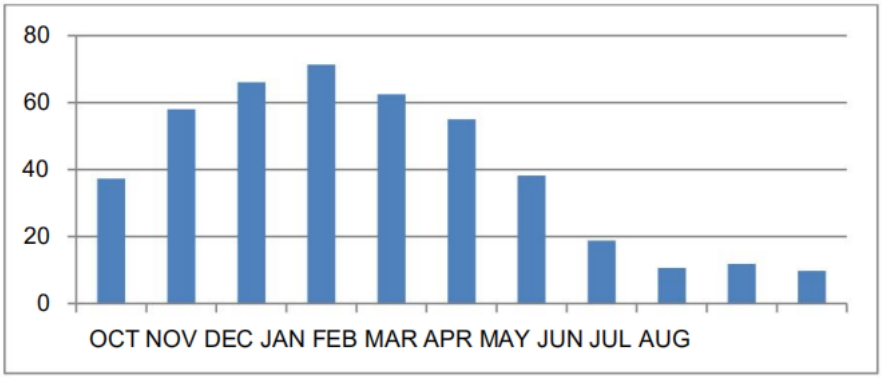

Figure 4. Viskan's monthly average water flow at Kullagård (Modigh el al, 2012)

Converted to a return period, a 100-year high flow at Kullagård corresponds to approximately 168 m^3/s. Regarding low water flows, a 100-year low flow corresponds to approximately 3 m^3/s based on data for the entire year. If the same calculation is carried out only for August, the 100-year low water flow corresponds to approximately 2.5 m^3/s (Modigh el al, 2012).

According to Engdahl and Pile (2019), precipitation is estimated to increase by 10-30% at the end of the century, mainly during the winter months. With regard to Viskan, it is possible to obtain a larger increase in precipitation in the northern parts of the catchment area. The increase then decreases to the south in the catchment area. In Viskan, the current 100-year flow, is expected to return more often between the years 2071 and 2100 compared with the reference period (1961–1990). Climate calculations also show flow changes at different times of the year, where it can be seen that there is an increased total average inflow with increased flows in winter and reduced flows during spring and summer.

The maximum water levels in the sea along the coast of Varberg are measured at 1.5–1.75 meters above the current average water level in extreme winds of 20-30 m/s. This can be compared with the average water level at Ringhals, which was measured at storm Gudrun in 2005 at 1.63 meters above the average water level. A possible increase in sea level of 1 meter would thus mean a sea level of 2.5–2.75 meters above the current average water level at the end of the century in extreme winds (Engdahl and Pile, 2019).

2.3 River Hydraulics

The roughness characteristics may differ significantly over a cross-section due to thick vegetation in overbanks with large trees shown as the Figure 5. The different roughness conditions cause different frictional resistances against the water flow which imply different Manning's value in the model. In general, a river with higher roughness causes a higher energy loss compared to a river with lower roughness (Brunner, 2021).

Figure 5. A river section of Viskan with large trees at the overbanks at downstream

Besides surface roughness, the irregularities in shape and size of the Viskan sections can influence on the frictional energy loss. Moreover, the sea water level variation at outlet has significant impact on the flow velocity and causes backwater effects.

2.4 Geomorphology and Sediment Transport

The morphology of the bedrock constitutes a fissure valley landscape and has primarily been influenced by the development during the Mesozoic which is a geological era 245-65 million years ago. The rock is split into fissure valleys, which follow a relatively clear pattern (Figure 6). Central in the figure is Viskan's valley, which is oriented in the northeast-southwest (Engdahl and Pile, 2019).

The westernmost parts of Viskan's valley became ice-free about 14500 years ago. During the melting of the ice, the earth's crust became far below sea level, which meant that the sea covered very large parts of the landscape. Therefore, after the ice left the area, the soil crust was raised relatively quickly. Meanwhile, sea levels were also raised because all the meltwater was brought to the sea. This has created a gradual change in the level of the sea shore which is still ongoing. The changes in the landscape that have taken place are shown here with a series of beach level maps produced with a model developed at SGU shown from Figure 6 to Figure 9 (Engdahl and Pile, 2019).

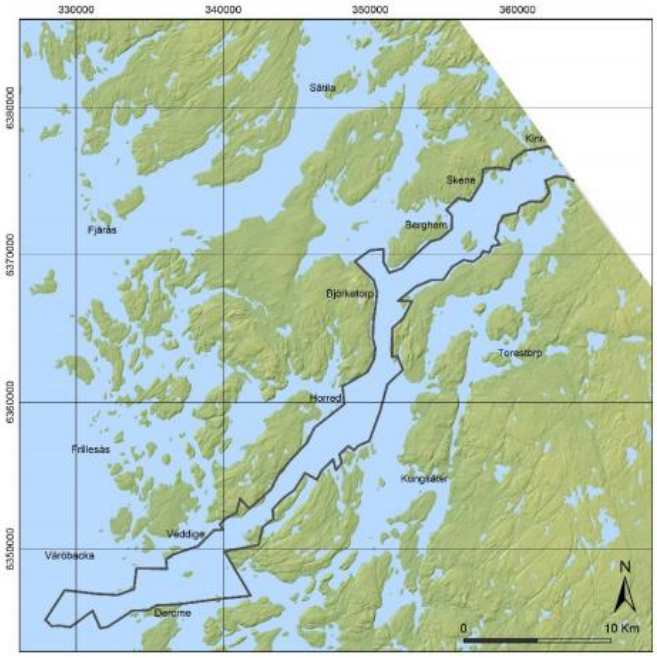

Figure 6. The distribution of land and water about 13,800 years ago when the ice sheet still remained in the northeastern part of the area (upper right corner)

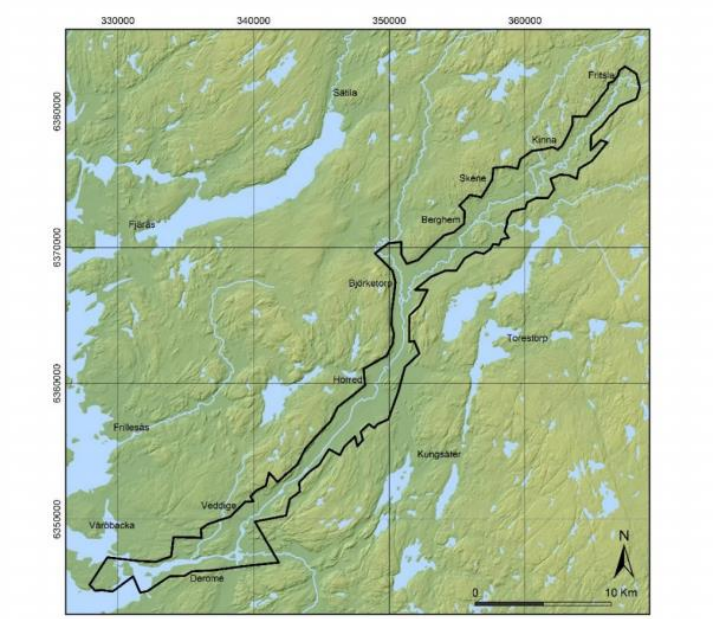

Figure 7. Distribution of land and water about 10,000 years ago

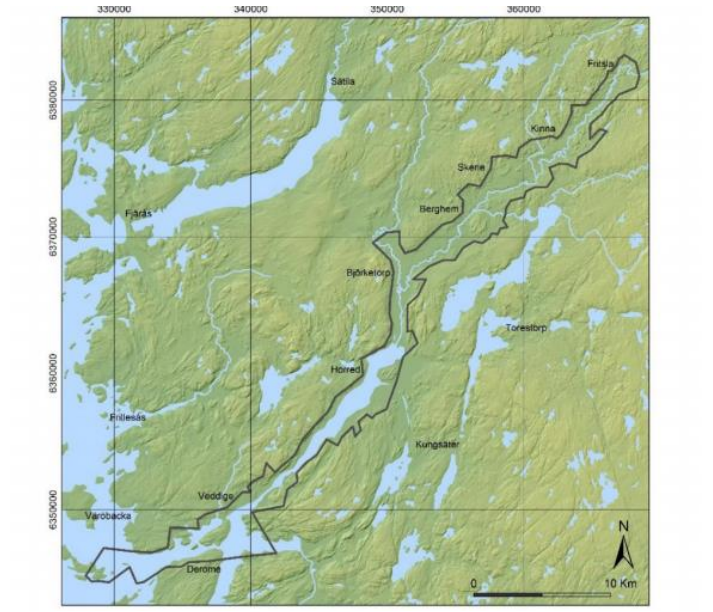

Figure 8. Distribution of land and water about 8600 years ago at the time of the maximum postglacial transgression

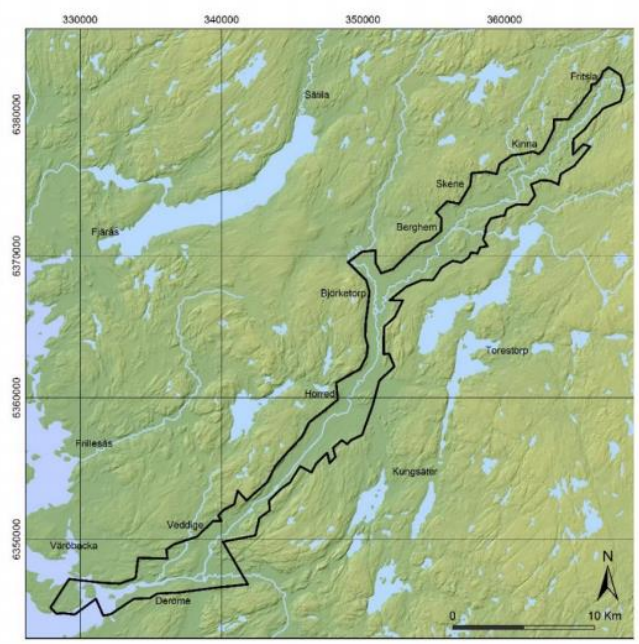

Figure 9. Distribution of land and water about 2000 years ago.

From about 8000 years ago until today, the shoreline has taken on lower levels. For about 2000 years then the sea surface was again about 2m above the current sea surface (Figure 8). The current land uplift in the area is about 2.5 mm/year (Engdahl and Pile, 2019).

Therefore, the glacial clay which makes up the bulk of the fine-grained sediments in the Viskan Valley was deposited during the melting of ice and for a time thereafter in an Arctic Sea for a period of about 4000 years. Figure 10 shows the soil type map in the valleys of Viskan (Engdahl and Pile, 2019).

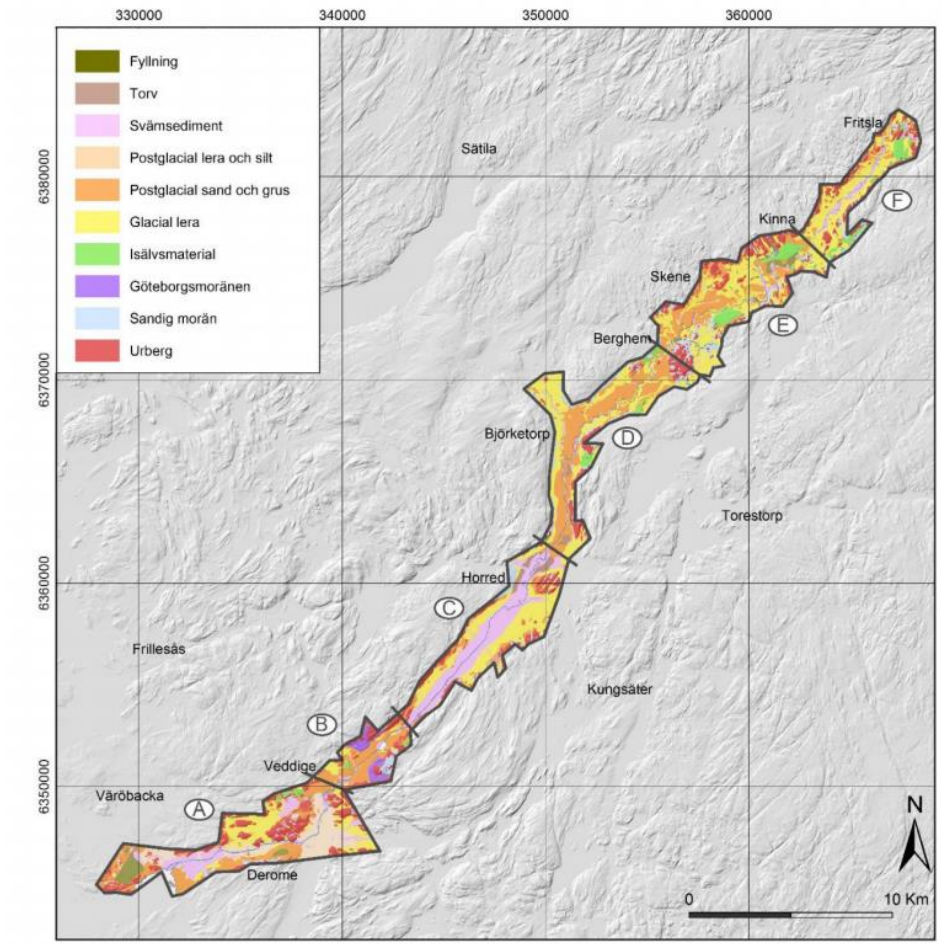

Figure 10. Soil type map in the valleys of Viskan and Häggån (Engdahl and Pile, 2019)

2.5 River Bank Erosion and Scour

Through SGI (Statens Geotekniska Institut) the river bank erosions of Viskan has been identified as a major challenge. The erosion occurs when more sediment is transported downstream than coming from upstream to the banks and bed in a particular area. The erosion is very significant at steep river sections, outer bend curves and close to the bridges where the water velocities are high or the flow path is changed in the Viskan. The red arrows and dots in Figure 11 shows locations with traces of landslides and ravines in soil layers as detected by SGI.

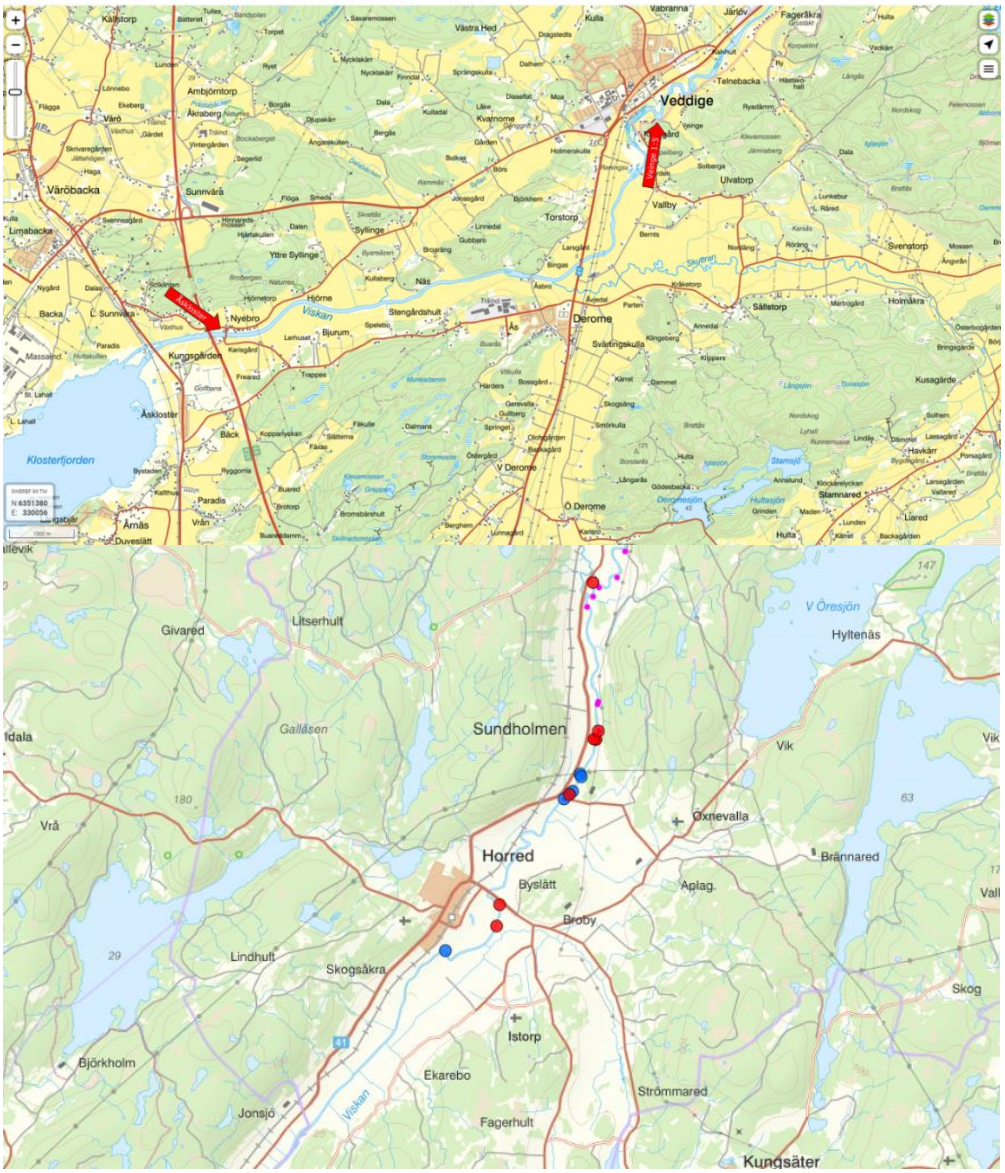

Figure 11. Locations with bank erosion and scour along Viskan (Rankka, 2022)

In the Viskan, there is no measured data on the sediment transport, but the river shows clear signs of erosion as seen in Figure 12 which shows one of the eroded zones along Viskan. The eroding banks are clear signs of erosion due to sediment transport gradients.

Figure 12. An example of typical erosion problems at Viskan causing trees to fall into river at upstream

Figure 13 shows another typical erosion area at Viskan. Through information from the surrounding residents, this field has had significant erosion up to 4m deep at the old time, therefore they have filled the bank in 2006 by themselves, which alleviated the erosion problem to a certain extent but it is still a challenging problem for a long term.

Figure 13. One of typical erosion problems at Viskan at downstream

Figure 14 shows a house crack because of the land erosion at Viskan. This is because the erosion of the river bank cause an uneven foundations, which lead to a crack in the house.

Figure 14. One of typical erosion problems at Viskan causing a house crack at downstream

3 Sediment Transport

3.1 Grain Size

Rivers usually convey quantities of sediment that enables form their own morphology. Sediment particles' properties will have an effect on the sediment transport load. Therefore, grain size is an important element in sediment transport. If the grain size is coarse the sediment will be harder to move. If the grain size is very fine the sediment transport could possibly emerge as wash load. Through grain size sediment grains may be classified into clays, silts, sands, granules, pebbles, cobbles and boulders. The most common classification is the Wentworth scale shown as Figure 15.

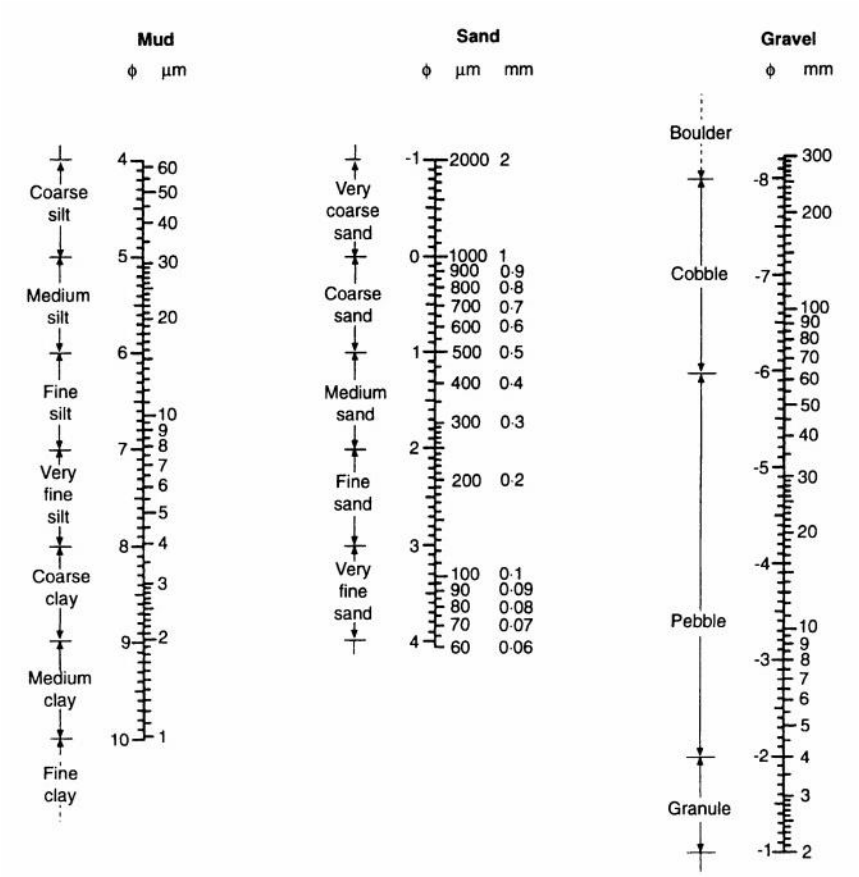

Figure 15. Conversion chart from phi units to microns (μm) and mm (Wentworth grain size scale) (Soulsby, 1997)

In nature most of the sediment is mixture with different grain sizes. It is difficult to present sediment by one grain size only. Therefore, the grain size distribution is normally presented by the mass of grains smaller than a certain diameter. In most cases the sediment is characterized by its median sieve diameter d_{50}, which means the diameter for 50% of the grains by mass is finer shown as in Figure 16. Likewise, d_{90} and d_{10} are sediment sizes for which 90 percentage and 10 percentage of the material are finer respectively (Soulsby, 1997).

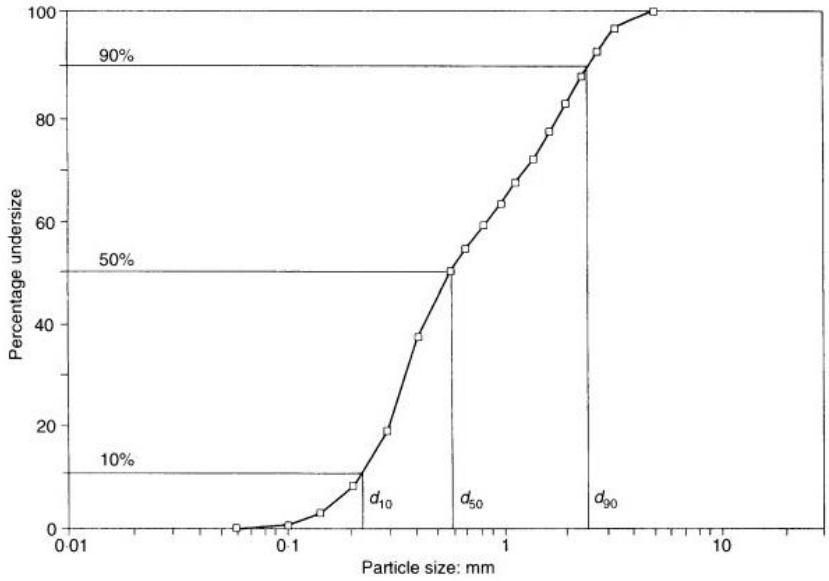

Figure 16. Example of grain size distribution (Soulsby, 1997)

3.2 Types of loads

When the shear stress exceeds the threshold of motion the sediment begins to transport. There are three forms of sediment transport called bedload, suspended-load and wash load transport. Figure 17 shows the difference between bed load and suspended load.

Bedload transport is movement of sediment particles along the bottom of the river. For bedload transport the shear stress is the essential factor. Grains could be rolling, sliding and hopping along the bed. Bed load occurs when flow is slow and over flat beds or in conjunction with ripples for stronger flows or flows is very strong over a flat bed. Therefore, bed load dominates for low flows or large grains (Soulsby, 1997).

Suspended load is the sediment transport when sediment particles are suspended in the water column due to turbulence. This is the sediment particles when the shear stress is increased and causes them to become suspended. Therefore, we can develop the sediment concentration profiles to determine the suspended load (Soulsby, 1997).

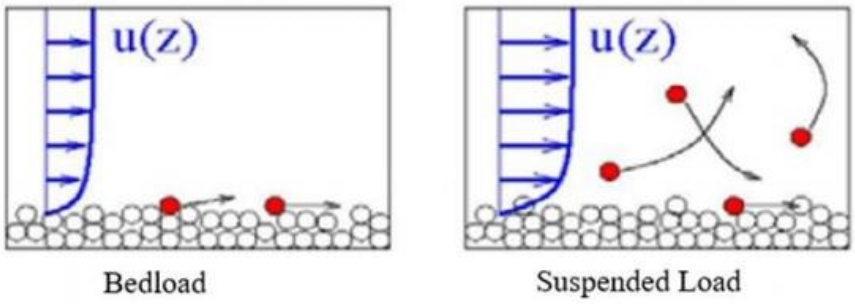

Figure 17. Bedload and suspended load as a result of initiation of motion (Carmenen and Larson, 2007)

3.3 Process and mechanism

In sediment transport studies, there are critical small-scale processes controlling sediment transport which are related to bottom boundary layer dynamics. Boundary layer is the layer of water in the immediate vicinity of the bounding surface where the effects of viscosity are significant (Soulsby, 1997).

The forces acting on a particle are a forward force due to its drag F_D, the lift force F_L, submerged weight W_S, and resistance force F_R as shown in Figure 18 (Yang, 2006). The direction of the drag force is influenced by the direction of the particle velocity (v), which relative to the flow (Rijn, 1984).

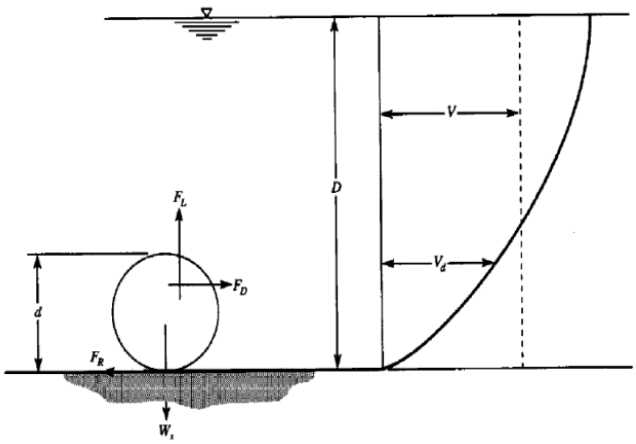

Figure 18. Showing the forces acting on a spherical sediment particle at the bottom of an open channel (Yang, 2006)

There are two flow parameters which are the shear stress and velocity, which can influence forces or moments. The shear stress, the different in density between the sediment and fluid, the diameter of the particle, the kinematic viscosity and gravitational acceleration are important factors and need to be considered. For a uniform flow, this can be expressed as follows:

$$\tau = \gamma RS \tag{1}$$

Where:

τ = average shear stress (Pa)
γ = specific unit weight of the water (N/m^3)
R = hydraulic radius
S = surface slope of water

The threshold of motion is the critical value of sediment transport, which is an important factor when determining the sediment response to currents. When the flow velocity is slow enough over a sand bed the sand will be immobile. If the flow velocity increases to a certain value a few grains will begin to move. This is called the threshold of motion or incipient motion (Soulsby, 1997). The threshold bed shear stress τ_{cr} can be formulated as

$$\theta_{cr} = \frac{\tau_{cr}}{g(\rho_s - \rho)d_{50}} \tag{2}$$

Where:

τ_{cr} = threshold bed shear stress (Pa)

g = acceleration due to gravity (m/s^2)

ρ_s = the density of the sediment (kg/m^3)

ρ = the density of water (kg/m^3)

θ_{cr} can be formulated through

$$\theta_{cr} = \frac{0.3}{1 + 1.2D_*} + 0.055\left(1 - \exp(-0.020D_*)\right) \quad (3)$$

Where:

D_* is dimensionless grain size can be calculated by:

$$D_* = \left(\frac{g(s-1)}{v^2}\right)^{1/3} d_{50} \quad (4)$$

Where:

s = $\rho_{sediment}/\rho_{water}$

The most widely used analyses for incipient motion are derived from the shear stress approach. In HEC-RAS model, the shield's diagram approach is employed for particle incipient motion. Figure 19 shows the diagram produced by shield used in HEC-RAS (Brunner, 2021).

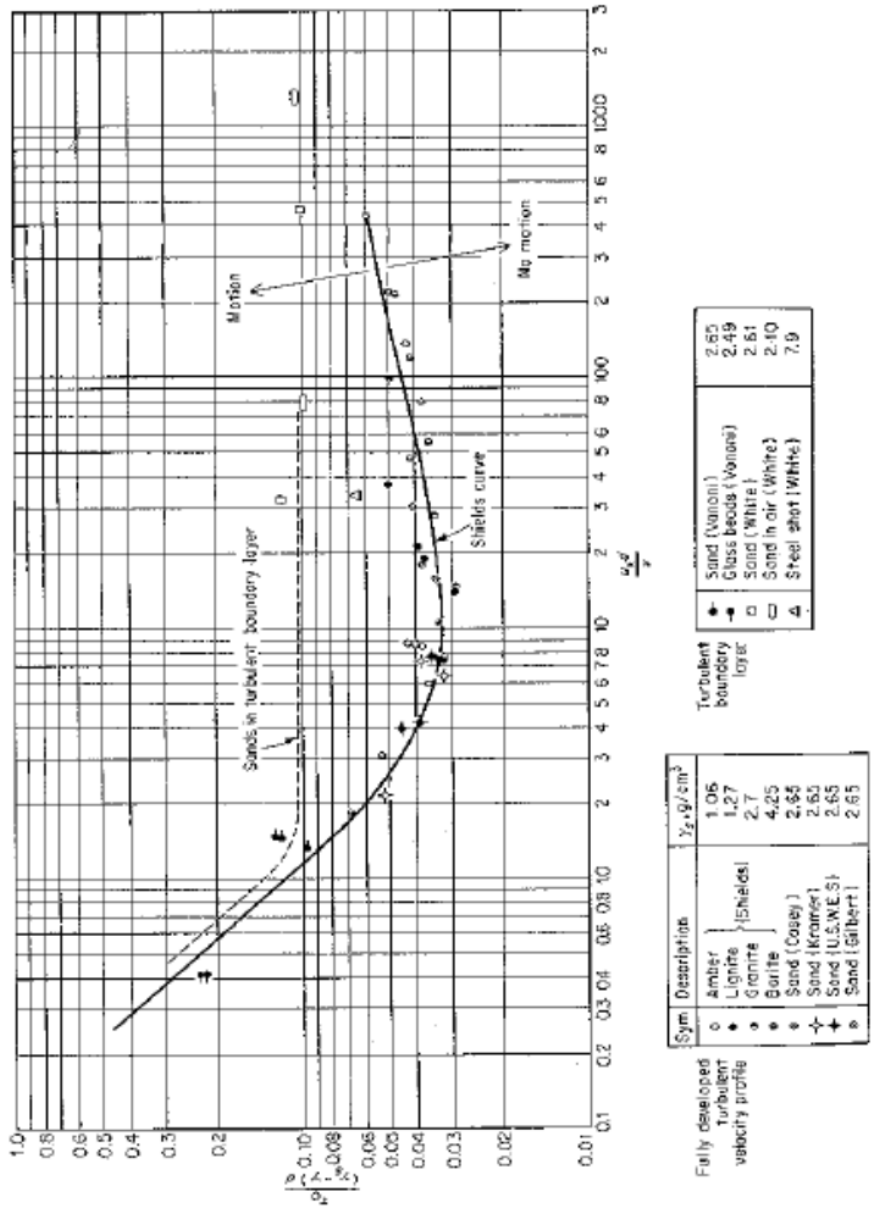

Figure 19. Shield's diagram, Graf (1971) considered for incipient motion in HEC-RAS (Brunner, 2021)

3.4 Slope failure and bank stability

Sediment transport from riverbanks often cause slope failure as the mass of soil is transported resulting from forces that do not balance. The different types of slope failure known are plane, wedge, toppling, rockfall and rotational that is circular and non-circular (Hoek and Bray, 1981). Figure 20 below shows common types of slope failure.

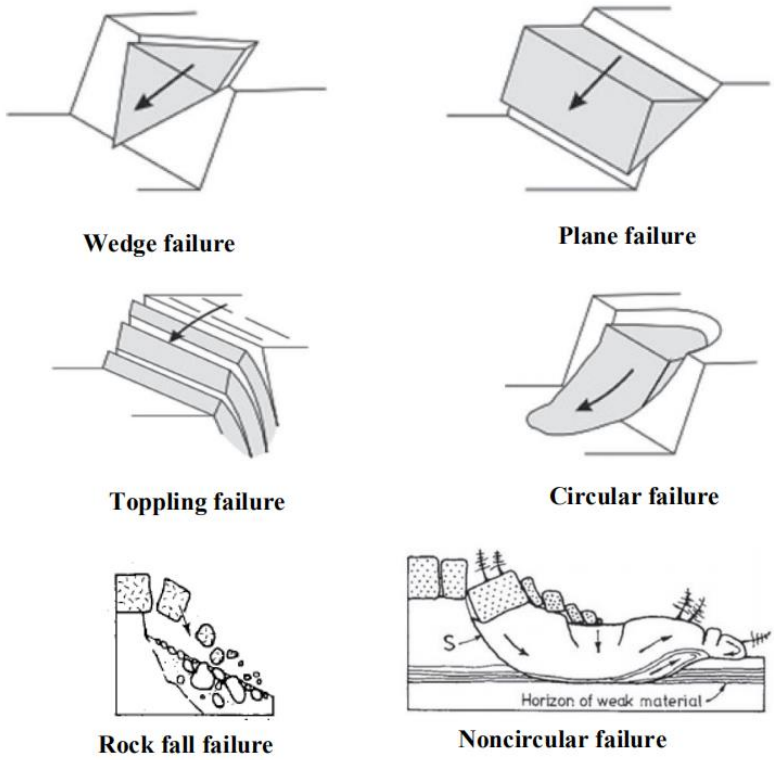

Figure 20. Types of slope failures (Hoek and bray, 1981; Blyth and de Freitas, 1984)

Plane, wedge, toppling and rockfall are common in rock formations and the main controlling factor is the orientation and spacing of discontinuities in the planes relative to the slope. Rotational failures (circular or non-circular) are common when the materials are soils, mine dumps, heavily jointed or fractured rock mass and very weak rocks. The key controlling factor for these failures is the material properties, water content and foundation strength (Rai & Singh, n.d.).

4 The HEC-RAS model

The Hydrologic Engineering Center's River Analysis System, generally known as HEC-RAS is an open-source computer-aided program developed by the US Army Corps of Engineers at the Hydrologic Engineering Center in Davis California. This software was developed to be employed for various useful river analysis such as one-dimensional steady flow, one and two-dimensional unsteady flow, sediment transport, water temperature and water quality, and bridge scour. The model can perform calculations for both prismatic and natural channels (Brunner, 2021).

The software mainly consists of four main river analysis components. First of all is the steady flow water surface profile computations, the second is unsteady flow simulations done as one or two-dimensional hydrodynamics, the third one is quasi-steady or fully unsteady flow movable boundary sediment transport computations done also as one or two-dimensional and the last is water quality analysis. A common factor for all the four simulations components is that all use of the same geometric data representation and same geometric and hydraulic computation routines. Additionally, the model contains some hydraulic design features that can be used once the water surface profiles are computed (Brunner, 2021). For this case, the current model study is performed by a 1D steady flow analysis with sediment transport computations. The two features are explained in the following subsections.

4.1 Steady flow

In steady flow, one of the important aspects to be determined is the water surface profile from one cross section to another. It can be achieved by solving the energy equation by standard step method. The energy equation considered from one point to another is written as:

$$Z_2 + Y_2 + \frac{a_2 V_2^2}{2g} = Z_1 + Y_1 + \frac{a_1 V_1^2}{2g} + h_e \qquad (5)$$

Where:

Z_1 and Z_2 = elevation of the main channel inverts (m)
Y_1 and Y_2 = depth of water at cross sections (m)
V_1 and V_2 = Average velocities at cross sections (m/s)
a_1 and a_2 = Velocity correction coefficients
g = acceleration due to gravity (m/s^2)
h_e = energy head loss (m)

The terms of the energy equation are depicted in Figure 21.

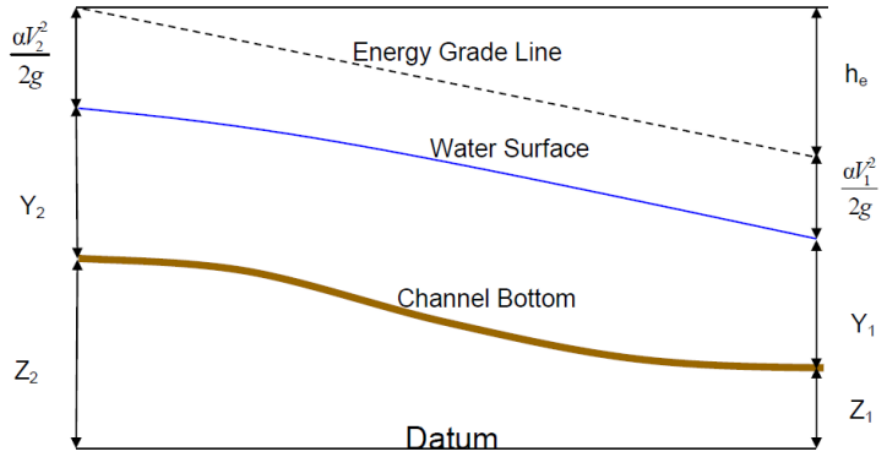

Figure 21. The graphical representation of the energy equation (Brunner, 2021)

The energy head loss h_e between two cross sections constitutes the friction losses and contraction or expansion losses. It is written as follows:

$$h_e = L\bar{S_f} + C\left|\frac{a_2V_2^2}{2g} - \frac{a_1V_1^2}{2g}\right| \quad (6)$$

Where:

L = discharge weighted reach length (m)
$\bar{S_f}$ = representative friction slope between two sections
C = expansion or contraction loss coefficient

The distance weighted reach length L, is calculated through the following equation:

$$L = \frac{L_{lob}\overline{Q_{lob}} + L_{ch}\overline{Q_{ch}} + L_{rob}\overline{Q_{rob}}}{\overline{Q_{lob}} + \overline{Q_{ch}} + \overline{Q_{rob}}} \quad (7)$$

Where:

L_{rob}, L_{ch}, L_{lob} = reach lengths of cross-sectional flow in the left overbank, main channel and right overbank

$\overline{Q_{lob}}$, $\overline{Q_{ch}}$, $\overline{Q_{rob}}$ = mean of the flow between sections for the left overbank, main channel and right overbank

The friction slop is calculated as:

$$\bar{S_f} = \left(\frac{Q_1 + Q_2}{K_1 + K_2}\right)^2 \quad (8)$$

Where:

Q_1 and Q_2 = flows at the two cross sections (which is the same for steady flow)

K_1 and K_2 = conveyance at the two cross sections which is given as:

$$K = \frac{1}{n} AR^{2/3} \quad (9)$$

Where:

n = Manning's coefficient of roughness

A = cross sectional flow area

R = Hydraulic radius

The continuity equation is also employed to solve for the velocity and water surface profile which is shown as follow:

$$Q = A_1V_1 = A_2V_2 \quad (10)$$

Where:

Q = river flow

A = sectional area

V = flow velocity

The continuity equation above produces the same flow at any location along the river.

Boundary conditions are important to form initial water surface profiles at both the upstream and downstream end of the river system. HEC-RAS is capable of calculating water surface profile for subcritical, supercritical and mixed flow in steady flow simulations. In a subcritical flow regime, boundary conditions are only essential at the downstream end of the river. For a supercritical flow regime, boundary conditions are essential at the upstream end. As for a mixed flow regime, boundary conditions must be entered at both upstream and downstream of the river reach (Brunner, 2021). Boundary conditions in a steady flow profile include:

- Known water surface elevations
- Critical depth
- Normal depth
- Rating curve

4.2 Sediment transport

Within HEC-RAS it is possible to perform one-dimensional and two-dimensional sediment transport analysis. In this study the one-dimensional sediment transport analysis is considered. HEC-RAS includes mobility boundary, sediment transport modelling capabilities which influence sediment and modify channel cross sections responses to sediment dynamics. Although HEC-RAS has the great abilities of sediment transport modelling, the modelling of sediment is not easy, especially because the uncertainty of some sediment data and the transport theory is empirical and sensitive (Gibson and Sánchez, 2020). In order to simulate the sediment transport in HEC-RAS the river geometry, quasi-unsteady flow with temperature and sediment data file are needed as shown in Figure 28 in chapter 5.

4.2.1 Sediment continuity equation

According to Gibson and Sánchez (2020), the Exner equation is employed in HEC-RAS sediment model. Below is the Exner equation as presented HEC-RAS 1D sediment manual:

$$(1-\lambda_P)B\frac{\partial \eta}{\partial t} = -\frac{\partial Q_S}{\partial x} \tag{11}$$

Where:

B	= Channel width
η	= Channel bottom elevation
T	= time
X	= distance
λ_P	= active layer porosity
Q_s	= transported sediment load

The foundation of the HEC-RAS sediment transport calculations is the conservation of mass. The Exner equation states that the difference between sediment entering and leaving in a control volume must be stored or removed from the storage. It translates the difference between inflow and outflow loads into bed change, eroding or depositing sediment.

HEC-RAS solves the sediment continuity equation by computing the sediment transport capacity for control volume related to each cross section and comparing it with the sediment supply which entering the control volume. When the capacity is more than the supply, HEC-RAS meets the deficit by

eroding bed sediment, and when supply is greater than the capacity, HEC-RAS deposits the sediment and creates accumulation.

4.2.2 Transport functions

There are various transport functions in HEC-RAS and they can be chosen according to different needs. The most common parameter for selection of the transport function is the distribution of the grain size from a sieve analysis, because the transport functions have been developed for a range of grain size applications. In HEC-RAS sediment material is split into several grain classes. The range of transportable material in terms of grain size are from 0.002mm to 2024mm. There are seven different transport functions to choose from, and these are:

- Ackers and White
- Englund and Hansen
- Copeland-Laursen
- Meyer-Peter and Müller
- Toffaleti
- MPM-Toffaleti
- Yang
- Wilcock and Crowe

Most of sediment transport functions are based either on shear stress or stream power. The usually use an excess-shear or excess-power form, which compare the actual shear or power to a threshold. HEC-RAS does not compute any transport for the grain class if it is below the threshold (Gibson and Sánchez, 2020). The six shear stress or stream power equations are shown in Table 1:

Table 1: Transport functions based on excess shear stress and stream power (Gibson and Sánchez, 2020)

Excess Shear Stress	Excess Stream Power
Meyer-Peter and Müller	Ackers and White
Copeland-Laursen	Englund and Hansen
Wilcock and Crowe	Yang

The transport function adopted for this study is the Meyer-Peter and Müller formula which is a bedload equation developed from experiments of sand and gravel under plane bed conditions. The governing principle is that the transport rate is proportional to difference between the mean shear stress acting on the grain and critical shear stress. The range of applicable particle sizes is 0.4 to 29 mm and Darcy-Welsbach friction factor is employed to define bed resistance. In order to account for the finer material, the Krone and Parthenaides was included in the model sediment transport setup (Gibson and Sánchez, 2020). Below is the Meyer-Peter and Müller:

$$q_b^* = 8(\tau^* - \tau_c^*)^{3/2}, \tau_c^* = 0.047 \quad (12)$$

Where:

q_b^* = the Einstein bedload number (corrected with bedload)
τ^* = the Shield's stress
τ_c^* = the critical Shield's stress

More transport functions are used for comparison including Copeland-Laursen, Englund and Hansen and Wilcock and Crowe. Copeland-Laursen developed a total-load, excess-shear transport function with the form:

$$C = 0.01\gamma \left(\frac{d}{D}\right)^{\frac{7}{6}} \left(\frac{\tau'}{\tau_c} - 1\right) f\left(\frac{u_*}{\omega}\right) \quad (13)$$

Where:

C = concentration
D = the ratio of the representative partied size
D = water depth
u^* = the ratio of the shear velocity
ω = the fall velocity

Englund and Hansen is a total load transport equation which developed from flume data, using relatively uniform sand sizes between 0.19 mm and 0.93 mm. The equation is:

$$g_s = V^2 \left(\frac{\tau_b}{(\gamma_s - \gamma)d_{50}}\right)^{\frac{3}{2}} \sqrt{\frac{d_{50}}{g\left(\frac{\gamma_s}{\gamma} - 1\right)}} = V^2(\tau^*)^{\frac{3}{2}} \sqrt{\frac{d_{50}}{g\left(\frac{\gamma_s}{\gamma} - 1\right)}} \quad (14)$$

Where:

g_s	= sediment transport by unit width
γ	= unit weight of water
γ_s	= unit weight of sediment
V	= average channel velocity
τ_b	= bed shear stress
τ^*	= dimensionless shields number
d_{50}	= median particle size

Wilcock and Crowe is a bedload equation designed for well-graded rivers containing both sand and gravel. They define transport W_i^* as two functions of the dimensionless shear ratio $\frac{\tau^*}{\tau_{ri}^*}$:

$$W_i^* = \begin{cases} 0.002\left(\frac{\tau^*}{\tau_{ri}^*}\right)^{7.5} & if\ \frac{\tau^*}{\tau_{ri}^*} < 1.35 \\ 14\left(1 - \frac{0.894}{\sqrt{\frac{\tau^*}{\tau_{ri}^*}}}\right)^{4.5} & if\ \frac{\tau^*}{\tau_{ri}^*} \geq 1.35 \end{cases} \quad (15)$$

Krone and Partheniades experiments combine deposition and erosion respectively using the assumption that cohesive particles are too small that their behavior is primarily influenced by surface forces rather than gravity. The fundamental concept is that a floc will stick to the bed not like sand and gravel that sink to the bed. Meanwhile, Partheniades erosion observes whether the bed shear stress is adequate to overcome the electrochemical forces holding the grains together instead of using the bed shear stress capability to lift a grain particle off the bed. These two functions are used in HEC-RAS to calculate the deposition and erosion of cohesive sediments (Gibson and Sánchez, 2020). Below is the mathematical representation of the two equations and explanation of the terms.

Krone Equation:

$$\left(\frac{dC}{dt}\right)_d = -\left(1 - \frac{\tau_b}{\tau_c}\right)\frac{V_S C}{y} \quad (16)$$

Where:

C = concentration of sediment

t = time

τ_b = bed shear stress

τ_c = critical shear stress for deposition

V_s = fall velocity

y = water depth

Partheniades Equation:

$$\left(\frac{dm}{dt}\right)_e = M\left(\frac{\tau_b}{\tau_c} - 1\right) \quad (17)$$

Where:

m = mass of material in the water column

M = empirical erosion rate for particle scour

In HEC-RAS there are two shear stress thresholds that can be defined used that define three cohesive transport conditions, which are: Deposition, Particle Erosion and Mass Erosion. The two user defined thresholds as shown in Figure 22 are:

τ_c: Critical shear threshold for particle erosion

τ_{mw}: Critical shear threshold for mass erosion

Where $\tau_c \leq \tau_{mw}$.

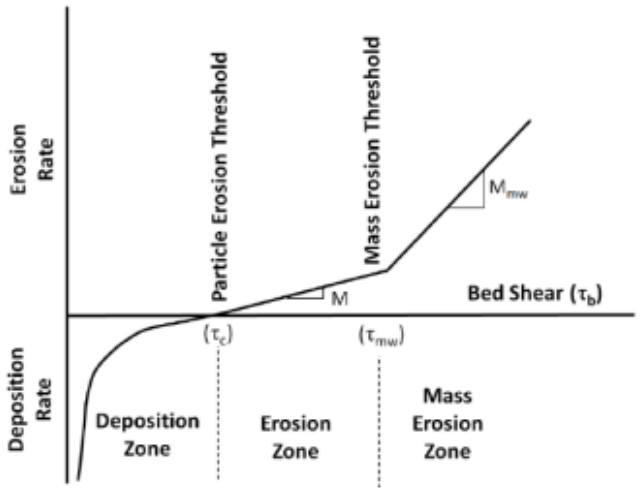

Figure 22. Diagram showing sedimentation zones and processes as a function of shear (Gibson and Sánchez, 2020)

HEC-RAS calculates the bed shear stress (τ_b) for every cross section and compares them to these thresholds (τ_c) and (τ_{mw}). The critical shear stress (τ_c) is mainly considered in computing if there will be erosion or deposition. Above this critical shear stress, as shown in Figure 22, there is erosion and below it there is deposition (Gibson and Sánchez, 2020).

The threshold values used for this study came from the experimental work by Partheniades (2009) on erosion of cohesive soils. It was done with mud from San Francisco Bay and the results are presented in Figure 23 below.

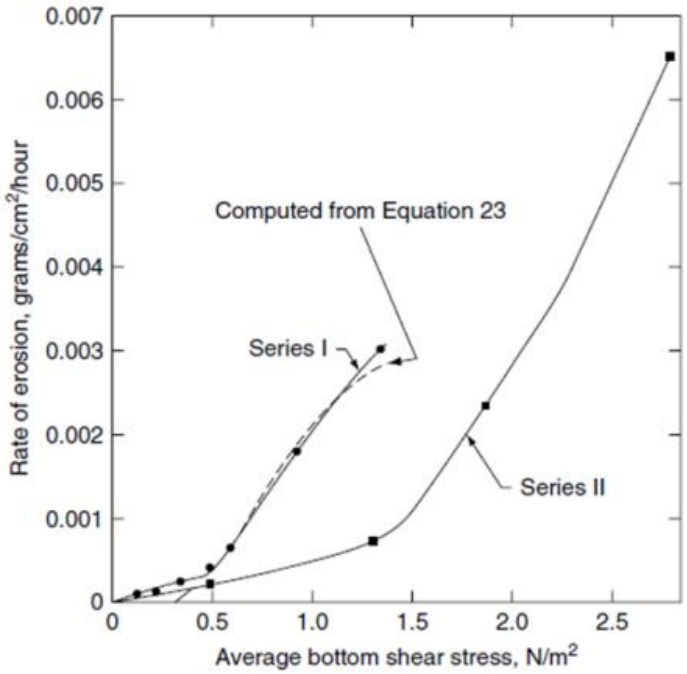

Figure 23. Shear stress rate of erosion for dense bed of San Francisco Bay mud (Partheniades, 2009)

From Figure 23, the results of two beds that were tested are presented. Beds with natural water content were studied in series I and in series II it was deposited beds generated by deposition as well as accumulation of suspended sediments at the bed due to low velocity. For this study, Series II was selected due to the reason that that a similar process occurs in the Viskan. In HEC-RAS, the values for τ_c and τ_{mw} used were 0 and 2 N/m^2 respectively, giving equivalent erosion rates 0 and 0.0028 grams/cm^2/hour.

4.2.3 Fall velocity

Fall velocity is used in Krone's deposition equation. Most fall velocity derivations begin with the balancing of the gravitational and the drag force on a particle descending on a water column for buoyancy as shown in Figure 24 (Gibson and Sánchez, 2020).

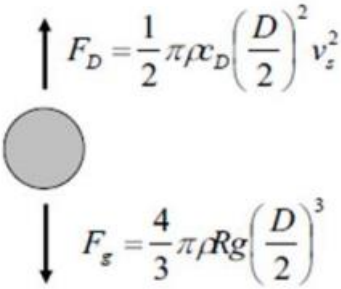

Figure 24. Free body diagram employed in calculating fall velocity with equations (Gibson and Sánchez, 2020)

Where:

F_D	= the drag force
F_g	= the gravitational force
ρ	= the density of the falling particle
D	= diameter of the falling particle
g	= acceleration due to gravity
C_D	= the drag coefficient
P	= density of water
V_s	= the fall velocity
R	= radius number

In HEC-RAS, there are seven fall velocity options that a user can select from and these are Rubey, Toffaleti, Van Rijn, Dietrich, Report 12, Soulsby and Wu and Wang. For this study, the Rubey fall velocity was selected since has shown to be adequate for silt, sand, and gravel grains (Gibson and Sánchez, 2020).

4.2.4 Sorting method

There are three algorithms to simulate bed sorting and armoring in HEC-RAS are available: Thomas (Ex5), Copeland (Ex7) and Active layer. These three algorithms split the bed into active and inactive layer. The active layer is a surface layer that corresponds to actively transporting material which means the material that could be transported. This is the layer that HEC-RAS

computes the transport capacity from. The transport capacity computation is based on the gradation of the active layer and not the whole bed (Gibson and Sánchez, 2020). Figure 25 illustrates the Exner 5 and Active layer.

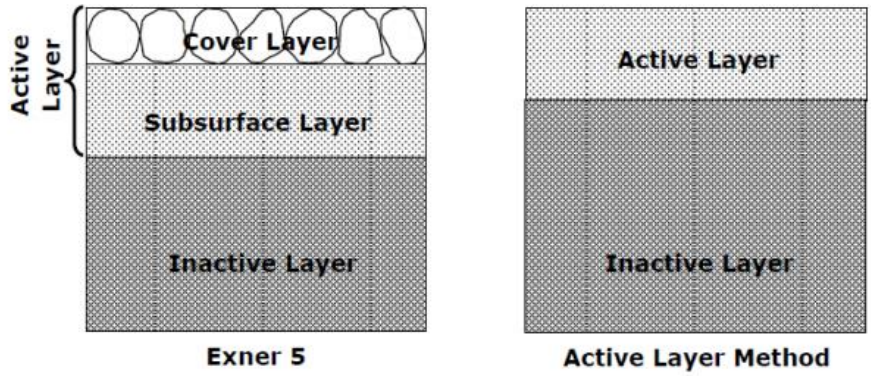

Figure 25. Schematic of the mixing layers in HEC-RAS sorting and armoring methods (Gibson and Sánchez, 2020)

In HEC-RAS, the Thomas mixing method formerly Exner 5 is the default sorting and armoring. Shown as Figure 25 this method is a three-layer bed mixing algorithm, which was developed to account for the influences of static armoring. The thin cover layer on top does not only regulates erosion but allows sediment to deposit on it and erode from it. When the model strips a grain class from it, HEC-RAS will try to satisfy the grain class transport capacity with the subsurface layer sediment (Gibson and Sánchez, 2020). For this study, this method has been chosen.

4.2.5 Quasi-unsteady flow

Hydraulic parameters are needed in sediment transport in HEC-RAS. Quasi-unsteady hydraulics is applicable to sediment studies. Its advantage is that the hydrodynamics are simplified and there is a representation of continuous flow with a series of discrete steady flow profiles which are even more stable. HEC-RAS splits these discrete steady flow profile (flow duration) which holds flow constant into computations increments which are further divided into bed mixing time steps (Gibson and Sánchez, 2020).

Over a particular duration HEC-RAS takes flow, temperature, stage and sediment to be constant (Gibson and Sánchez, 2020). Different flow duration can be set in HEC-RAS and for this study, the duration is set for 24 hours.

4.2.6 Computation increment

Computational increment is the main time step for quasi-unsteady hydraulic and sediment transport which subdivides duration and can be equal but not greater than duration. When conducting a sediment transport simulation in HEC-RAS, the flow for a particular duration remains unchanged until there is update of bed geometry and hydrodynamics during each computational increment. The computational increment is a sensitive and incorrect value which can influence the model to be unstable (Gibson and Sánchez, 2020). This was proven during the simulations of sediment transport. Figure 26 depicts how this works in HEC-RAS.

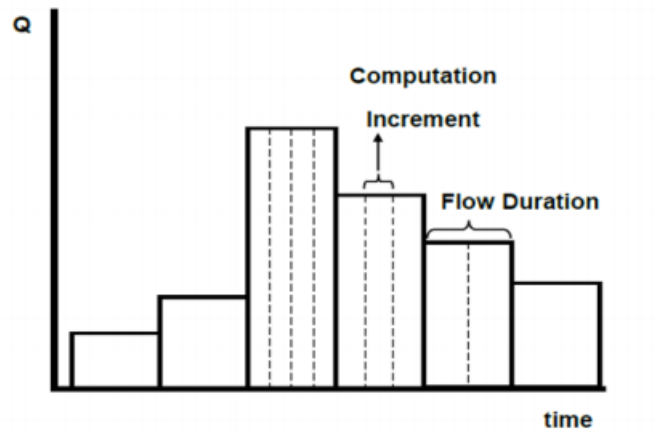

Figure 26. A quasi-unsteady flow file series with time step (Gibson and Sánchez, 2020).

4.2.7 Bed mixing time step

The bed mixing time step comes from the subdivision of computational increment by HEC-RAS. The model updates the composition of the bed mixing layers at the mixing time step unlike the computational increment where the hydraulic parameters and cross section elevation are held constant by HEC-RAS. The results are a revision of the grain class accounting in the layers several times between hydraulics and sediment capacity computations. Also, the vertical gradation profile adjusts in response to deposition and erosion even when there is no change in the bed until the end of the computational increment (Gibson and Sánchez, 2020).

4.2.8 Boundary conditions for sediment transport

Sediment boundary conditions included with HEC-RAS include rating curve, sediment load series, equilibrium load and clear water (no sediment). Rating curves give the sediment load with the corresponding flow at the point of measurement and can be used for cross sections with available sediment and flow measurements. Sediment load series is a sediment load that is not tied to a flow boundary. Because this boundary is not tied to a flow measured sediment load can be used in any of the cross sections except the downstream one. Equilibrium load is a condition set that sediment load equals the capacity and due to this there will be no aggradation or degradation at the particular cross section. The clear water boundary condition is just a simple way to define a no-sediment boundary which for example can simulate a high trap-efficiency dam outlet (Gibson and Sánchez, 2020). Due to lack of sediment data for the Viskan this was set as an equilibrium load boundary.

4.3 Flow changes for steady, quasi-unsteady flow

When there is a flow change which is an additional flow at mid of the river system, the flow after the cross section where tributary joins are larger than the upper flows. In HEC-RAS there are different ways to deal with this either river reach for the tributary is added or flow changing is added directly. For steady flow, only one option for adding flow change is present which can be employed easily. However, for quasi-unsteady flow three options exist (Gibson and Sánchez, 2020). A list of the options for quasi-unsteady flow are:

- Uniform lateral flow
- Lateral flow Series
- Internal Stage BC

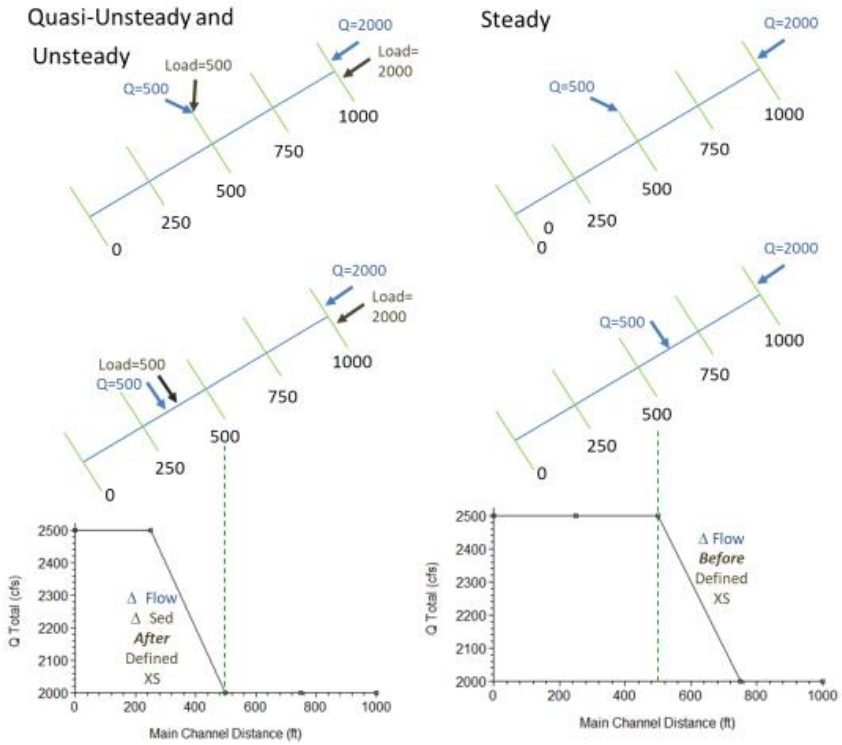

Figure 27. Schematic of flow change location associated with a lateral flow (Gibson and Sánchez, 2020).

Figure 27 illustrates the addition of a flow from a joining tributary. In this study, flow change was added in the steady flow simulation and for quasi-unsteady flow the later flow series has been applied.

5 Model Implementation

Input data used to simulate steady flow and quasi-unsteady flow for sediment transport in HEC-RAS software is summarized in the Figure 28 below.

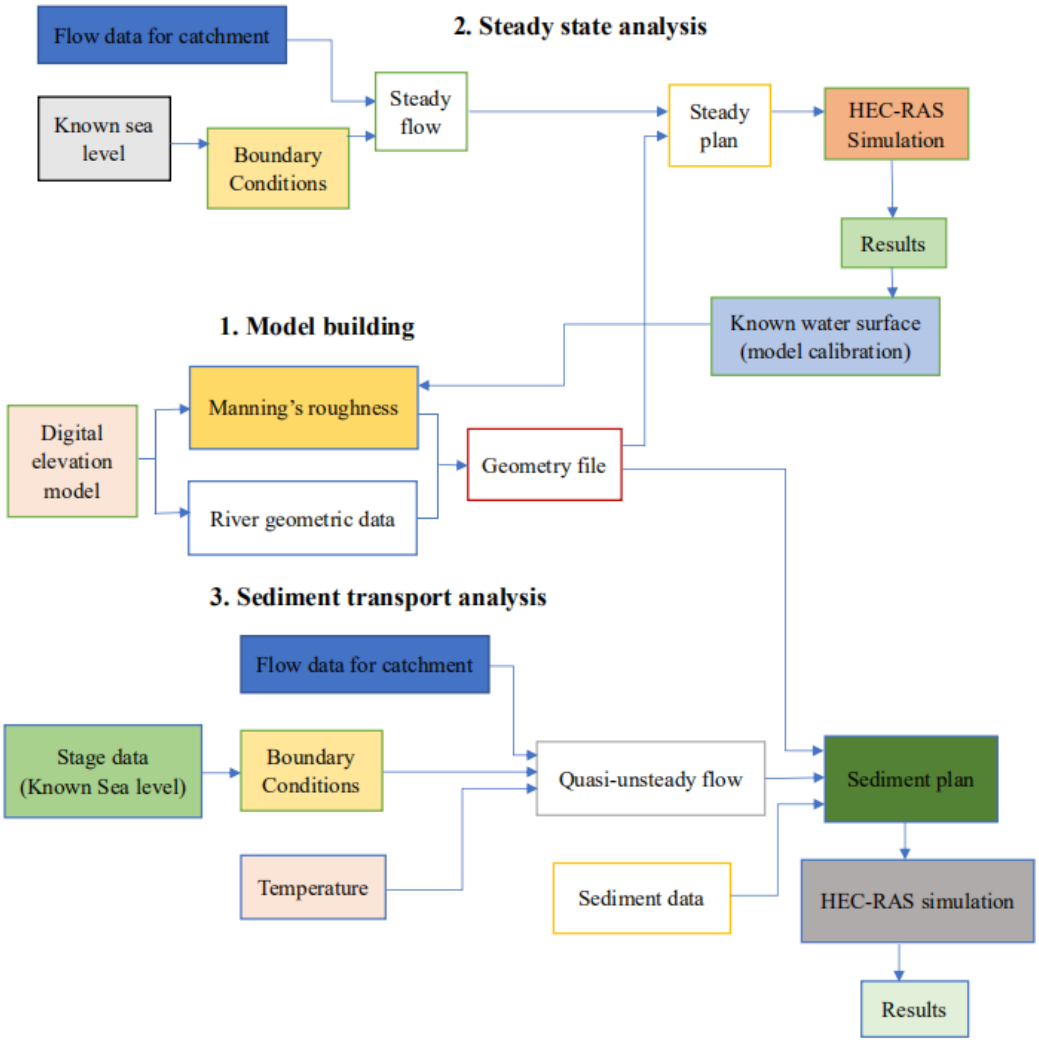

Figure 28. Flow chart of data used in HEC-RAS and how results are obtained from the simulation process.

Shown as Figure 28, the first step was to build a geometric model data that was used for the second step which was steady state analysis. Then, the same built geometric model also used for the third step which was sediment transport analysis. Moreover, the steady plan and sediment plan are simply the option in HEC-RAS that have the different input data files before simulation. This is selected in HEC-RAS by the user after all other files are ready.

5.1 Bathymetry of the river

The bathymetry data and topography of the study area came from SWECO (SWECO, 2014). However, the bathymetry data is more detailed at downstream river meanwhile the data for upstream is a bit rough which could influence the results of the model. According to SGI, there are deep erosion along the riverbed in certain stretches of the study area. This was also discovered during the model simulations, which was very important for this study.

To the Digital Elevation Model, river geometry including cross section, river reach, riverbanks, flow lines and flow paths were drawn in RAS Mapper found in HEC-RAS (see appendix 1). In HEC-RAS, the river reach was assigned 549 cross sections from upstream to downstream. Each cross section was automatically named by HEC-RAS using a specific number which increased from downstream to upstream. Figure 29 below shows all the assigned cross sections of the study area. A zoomed in view of cross sections is presented in Figure 1.1 of appendix 1.

Figure 29. Viskan with assigned cross sections in HEC-RAS Mapper

5.2 Sediment data

The sediment data was limited and there is no specific grain size distribution, therefore this study combined the information from County Administrative Board of Västra Götaland and SGU, then assumed a bed gradation which shows reliable results in sediment transport model. According to County Administrative Board of Västra Götaland and SGU the sediment is mostly fine with most grain sizes characterized between silt and sand shown as Figure 30. The sediment data could influence the sediment transport function selection to use for analysis as different functions were developed using grain size range. The grain size distributions are given in Table 2 adopted from HEC-RAS. Figure 31 presents the graphical results of the grain size distribution.

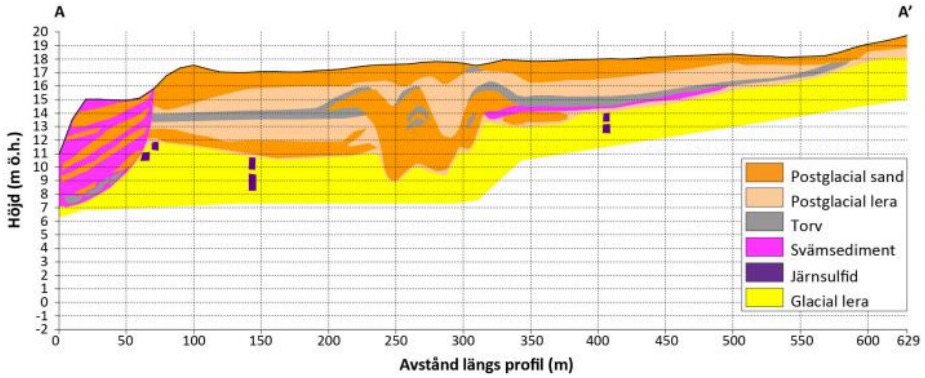

Figure 30. Bed gradation from part of Viskan (Norström, 2021)

Table 2. Grain size distribution

Grain classes	Grain diameter range	Sample
Clay	0.002-0.004	0
Very fine silt	0.004-0.008	0
Fine silt	0.008-0.016	0
Medium silt	0.016-0.032	0
Coarse silt	0.032-0.0625	0.5
Very fine sand	0.0625-0.125	0.66
Fine sand	0.125-0.25	8.68
Medium sand	0.25-0.5	24.86
Coarse sand	0.5-1	38.33
Very coarse sand	1-2	47.82
Very fine gravel	2-4	56.13
Fine gravel	4-8	69.49
Medium gravel	8-16	77.77
Coarse gravel	16-32	84.67
Very coarse gravel	32-64	90
Small cobbles	64	95
Large cobbles	128	98
Small Boulders	256	99
Medium Boulders	512	99.5
Large Boulders	1024	100

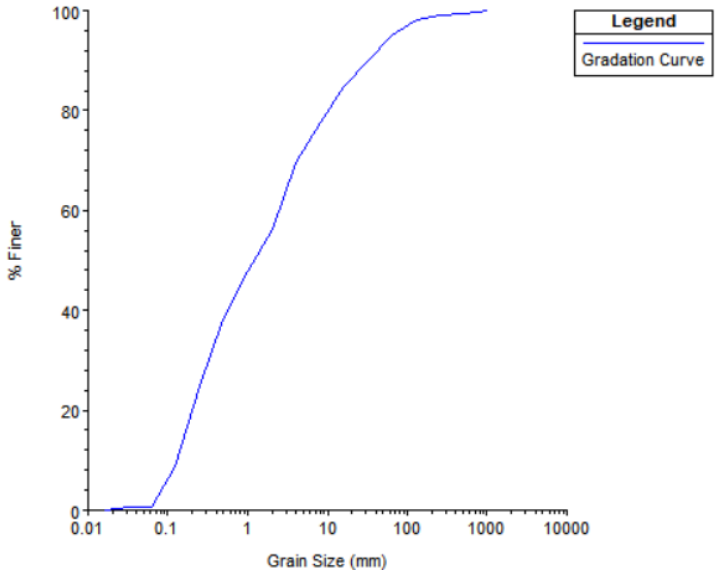

Figure 31. Grain size distribution for the sediment sample used in the study

5.3 Boundary conditions

In HEC-RAS, there is a need for a boundary condition for the last downstream cross section which have three options for users: normal depth, stage series and rating curve. Because the river ends up to the sea the downstream water level boundary condition of the river was considered as the sea water level. At 8 km from the downstream end of the river, there is an active station Ringhals, which has recorded a long time series of the sea water level from 1967 to 2022. In this study, stage data from 01st January 2012 to 31st December 2020 was used as input

The Ringhals station data from SMHI belongs to RH2000 which is one common elevation system, but the terrain elevation data from SWECO that this study was using for modelling was corresponding to RH00 which was not easy to change to RH2000. Therefore, this study models the river section with RH00 system by converting the SMHI sea level data with RH2000 into RH00 and use as boundary conditions. According to Lantmäteriet, the height difference at Ringhals is 0.138m shown as Figure 32 the map with reference points in the area around Varberg and height difference in meters between RH00 to RH2000. Figure 33 shows the average daily water levels for Ringhals station after conversion.

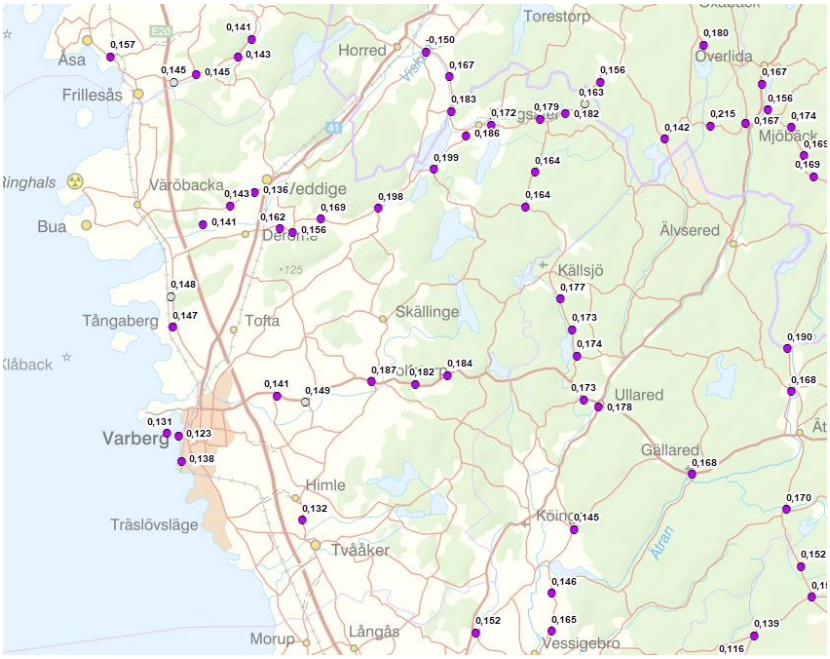

Figure 32. The map with reference points and height difference in meters between RH00 to RH2000

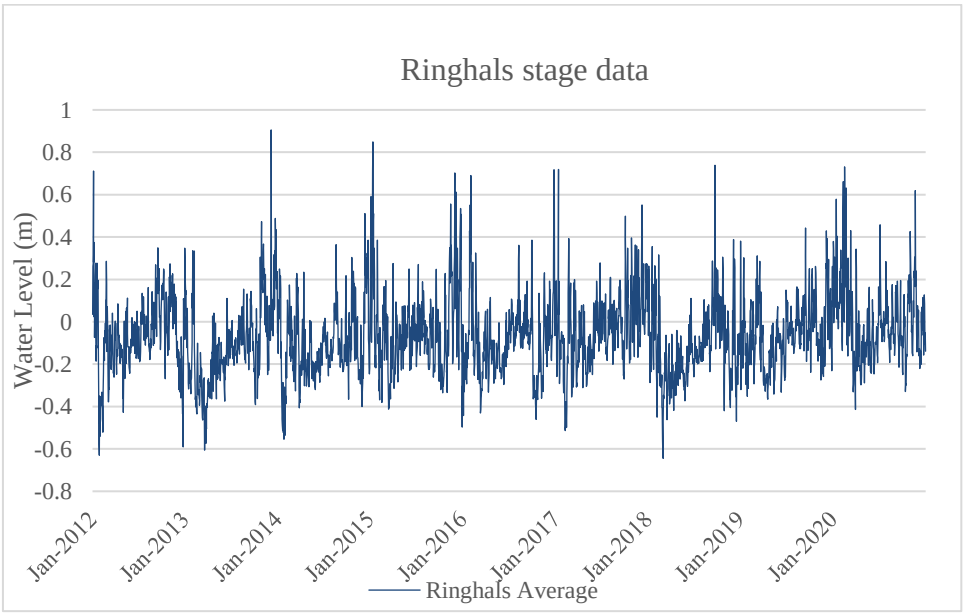

Figure 33. Calculated daily water levels for Ringhals station

5.4 Temperature data

Water temperature is important data in HEC-RAS that could influence the water viscosity. Water viscosity affects for sediment transport. At low temperature water has higher viscosity than at higher temperatures, which could increase sediment transport (Flynn, 2011). In HEC-RAS temperate data is required in the quasi-unsteady flow. In this study, temperature daily data were extracted from SMHI. The time series data obtained from 1st January 2012 to 31st December 2020. Figure 34 shows the temperature data series. From the data in Figure 34, the average temperature for the period of study is 9.3 °C.

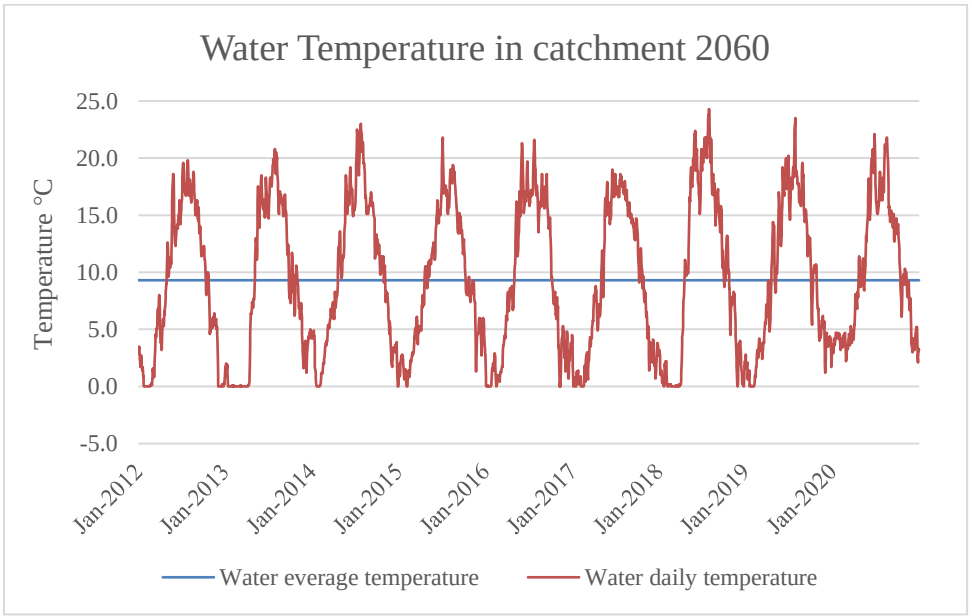

Figure 34. Water temperature at Viskan

5.5 Flow data of the river

HEC-RAS model requires flow data for both steady and quasi-unsteady flow simulation. It was important to have flow data for each catchment in the HEC-RAS model simulation. Flow data calculated for the years 2012 to 2020 was used in HEC-RAS that was extracted from SMHI for catchment 2383, catchment 2279, catchment 40002 and catchment 2060, as shown Figure 35. Average daily flow data for the study period from the year 2012 to 2020 in catchment 2383, 2279, 40002 and 2060 was calculated to be 31.8 m^3/s,

33.6m^3/s, 39.0m^3/s and 42m^3/s respectively. Table 3 shows average and maximum flows for catchment 2383, 2279, 40002 and 2060.

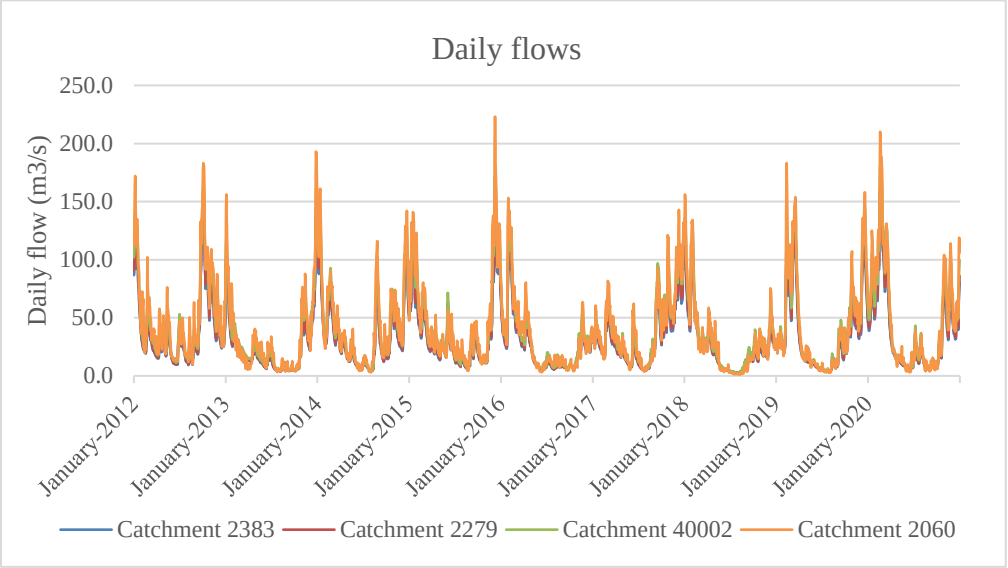

Figure 35. Daily flow data for catchment 2383, 2279, 4002 and 2060 from SMHI

Table 3. Average and maximum flows for catchment 2383, 2279, 40002 and 2060

	Catchment 2383		Catchment 2279		Catchment 40002		Catchment 2060	
Year	Annual average (m^3/s)	Maximum value (m^3/s)	Annual average (m^3/s)	Maximum value (m^3/s)	Annual average (m^3/s)	Maximum value (m^3/s)	Annual average (m^3/s)	Maximum value (m^3/s)
2012	39.2	135.0	41.4	141.0	48.2	162.0	51.7	183.0
2013	23.3	141.0	24.6	148.0	28.8	169.0	30.9	193.0
2014	34.2	117	36.0	123	41.7	141	44.5	161
2015	35.7	143.0	37.7	150.0	44.1	171.0	47.3	223.0
2016	24.6	107.0	25.9	112.0	29.8	125.0	31.6	153.0
2017	33.3	97.1	35.2	103.0	41.2	120.0	44.4	143.0
2018	24.5	111	25.8	117	29.9	136	31.8	156
2019	34.3	123.0	36.3	130.0	42.5	149.0	45.7	183.0
2020	37.9	156.0	39.8	163.0	45.9	183.0	48.8	210.0

In Table 3 the maximum value of flow in a year is the maximum 24h average flow for a day recorded during one year and the average flow is the average of all daily flows recorded in that year. It can be seen from the table the downstream catchment has higher flows than upstream catchment.

5.6 Calibration data

According to SWECO, the results of measurement of water levels along Viskan was used for HEC-RAS model calibration by modifying appropriate Manning's n value for Viskan. The data was recorded at 11st May 2014. Figure 36 shows the recording location at Viskan. The nine locations from upstream 37 to downstream 45 was used for this study area which are cross sections: cross section (XS) 96925, XS 86953, XS 45601, XS 33812, XS 24701, XS 21893, XS 5450, XS 4638 and XS 1722 in HEC-RAS corresponding to the locations in figure. Table 4 shows the water levels in the river recorded through SWECO.

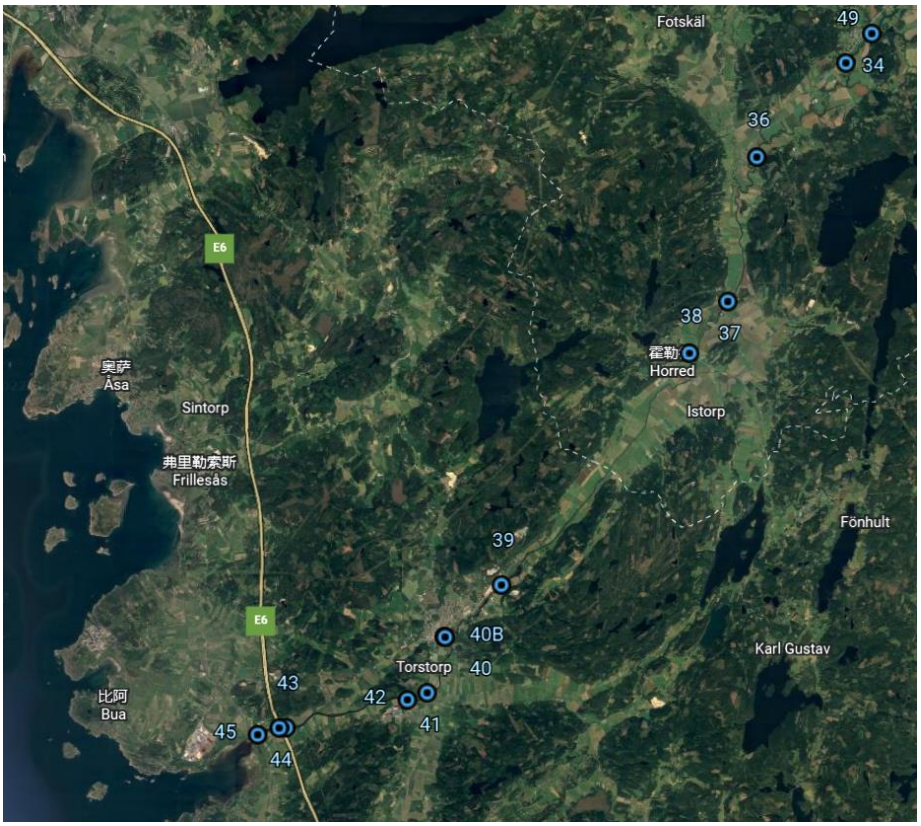

Figure 36. The measured locations along Viskan

Table 4. Water levels at Viskan at 11th May 2014 (SWECO, 2014)

Recorded location	Water level RH 00 (m)
37	9.81
38	8.7
39	6.45
40	3.32
41	1.19
42	1.18
43	0.08
44	0.06
45	0.04

As shown in Figure 33 and Table 4 recorded location 43, 44 and 45 is close to the river outlet to the sea. Therefore, the water level is close to the sea level. The calibration results are shown in chapter 6.1.

6 Model Simulation Results

In order to perform simulation with the model, the model structure was built up first. The bathymetry data was available so the calibration to establish the applicable Manning's n values for the left, right and main channel was the first step. This study was followed by two simulations: steady flow simulation and sediment transport simulation. The steady flow simulation was used to study the hydraulic parameters in the river and the quasi-unsteady flow was used to investigate the sediment transport with the sediment data editor.

6.1 Model Calibration

After the 549 cross sections drawn in the model, XS 96925, XS 86953, XS 45601, XS 33812, XS 24701, XS 21893, XS 5450, XS 4638 and XS 1722 were the cross sections corresponding the recorded locations shown in Figure 36. These were the focus cross section during the calibration. River water levels were recorded for 11st May 2014 which were used for the calibration. Finally, the attained Manning's values for the main channel were 0.07 and both the left and right bank of the channel were 0.08. The results obtained are presented in the Table 5 below. From the data in the Table 5, XS 33812 has the biggest error which is the place of the hydropower station. Because the lack of bathymetry data of the hydropower station, the model only considered the main channel of the river without the brunch of hydropower station channel. This might be the reason of the big error occurred at XS 33812.

Table 5. Water surface levels calibration

Cross sections	Flow (m^3/s)	Water level recorded (m)	Water level HEC-RAS (m)	Error (m)
96925	11.2	9.81	9.64	0.17
86953	11.7	8.7	8.78	-0.08
45601	13.1	6.45	7.03	-0.58
33812	13.1	3.32	2.21	1.11
24701	13.1	1.19	0.58	0.61
21893	13.1	1.18	0.26	0.92
5450	17.4	0.08	0.03	0.05
4638	17.4	0.06	0.02	0.04
1722	17.4	0.04	0	0.04

6.2 Hydraulic characteristics of the Viskan

After attaining the Manning's n values, a hydrodynamic simulation was conducted with calculated mean flow from catchment 2383 of 31.9 m^3/s applied from cross section 1109595 to 89076 after that catchment 2279 of 33.63 m^3/s applied from cross section 89076 to 52707 and catchment 40002 of 39.12 m^3/s applied from cross section 52707 to 13759 then another flow 41.86 m^3/s for the downstream catchment 2060 was used from catchment 13759 to 127, as shown in Figure 37. The downstream sea water level was set to an average water level of -0.067m and the selected type of flow was steady flow in HEC-RAS 6.1.0. The simulation results for the water surface, channel velocity and total shear stress are shown in Figure 38 to Figure 40.

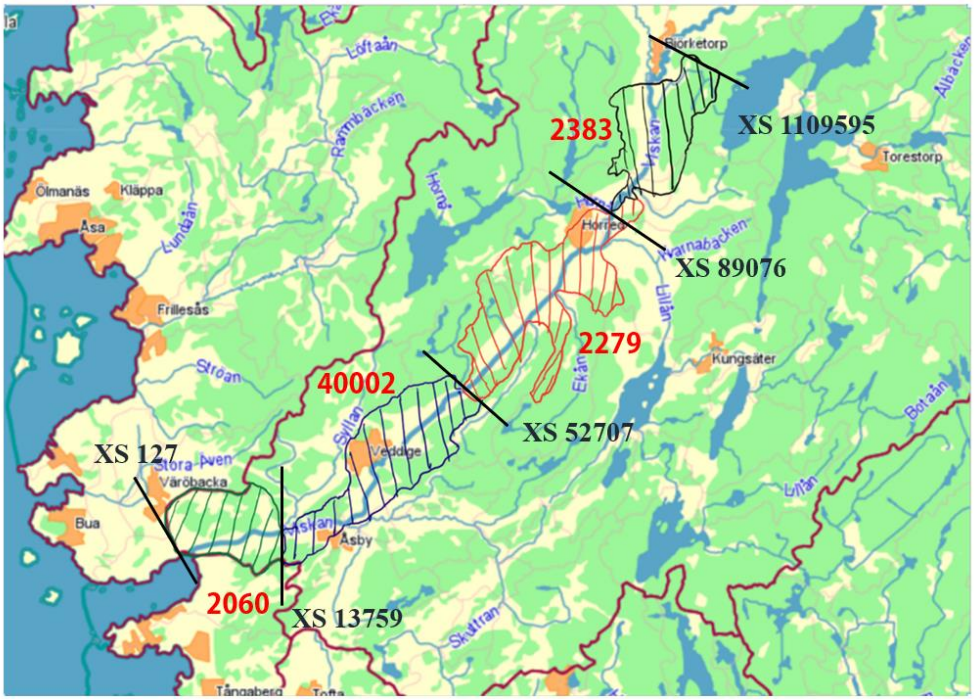

Figure 37. The sub catchment of Viskan with assigned cross sections

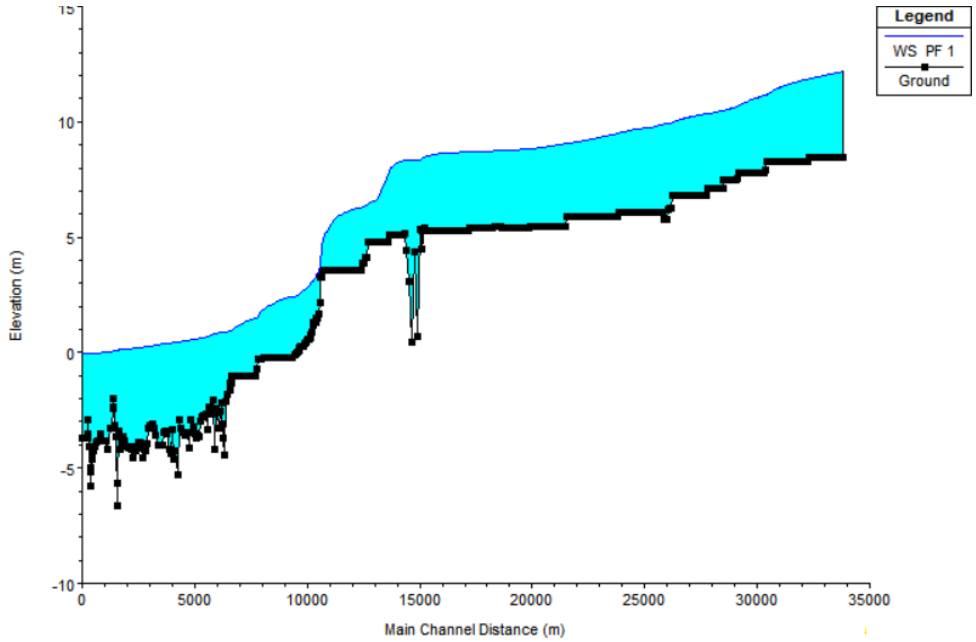

Figure 38. Water surface profile for the average flow simulation

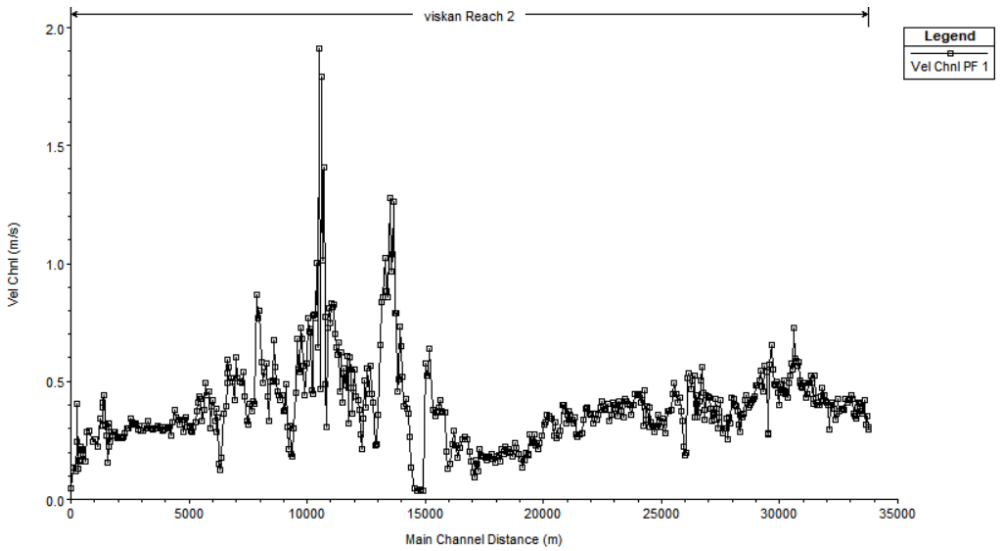

Figure 39. The channel velocity for the average flow simulation

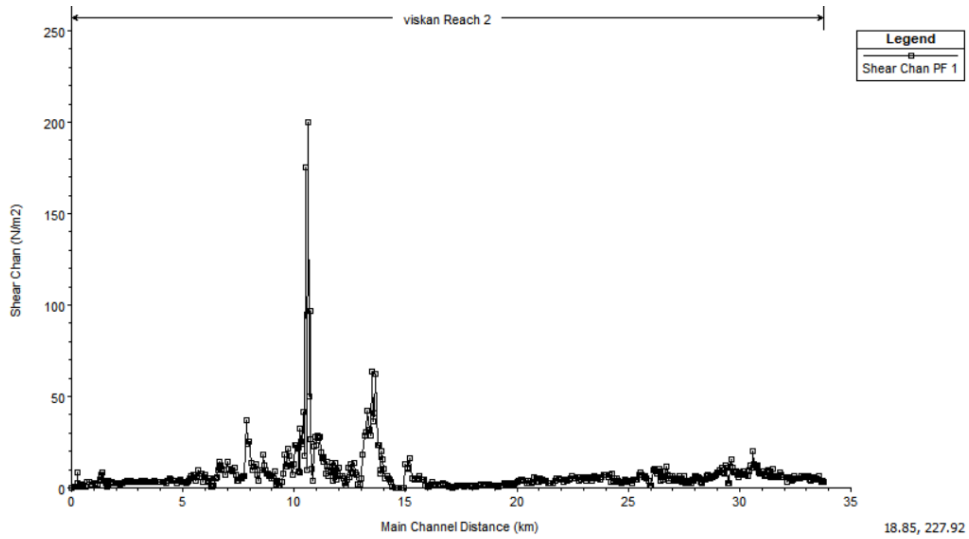

Figure 40. Total shear stress for the average flow simulation

From Figure 38, the highest water elevation from the steady state simulation was 12.16m at 33.78 km and reduces to 0.07m downstream. There is a big elevation drop around 10.6 km which is a hydropower station. This study only simulated the terrain of the main channel. Figure 39 shows that the lowest velocity in the study section of the river reach is at 14.92km which is 0.04 m/s. Other lower velocities show from Figure 39 is presented in the Table 6.

Table 6. Cross sections with low velocities

Cross section	Distance (km)	Low velocities (m/s)
127	0	0.05
5288	1.58	0.15
20828	6.31	0.12
49079	14.92	0.04
56202	17.09	0.09

In these cross sections the river widens but also from Figure 40, the same cross sections shows that the river goes deeper at these locations which decrease the velocities. Moreover, all the high velocities extracted from the Figure 39 are presented in the Table 7.

Table 7. Cross sections with high velocities

Cross section	Distance (km)	High velocities (m/s)
25883	7.85	0.87

34570	10.5	1.91
44377	13.49	1.28

From Table 7, the highest velocity is up to 1.91m/s at 10.5km which is the location of hydropower station. Cross section 25883 and 44377 had high velocities which is because the river become narrow at this section of river.

On the other hand, from Figure 40, the values for shear stress are also high at the location that the velocity is high. At cross section 25883 at 7.85 km the shear stress is 37.18 N/m^2, cross section 34570 at 10.5 km with 200.10 N/m^2 and cross section 44377 at 13.49 km with 63.8 N/m^2. Therefore, it can be found that the velocity is proportional to the shear stress. Both the velocity and shear stress are important for sediment transport.

6.3 Sensitivity analysis to determine worst case scenario

After having the trend of the hydraulic parameters, a sensitivity analysis at worst case scenario was conducted to understand how the varying sea water levels affects the velocity and shear stress. The flow was still the average flow. Results for this simulation for downstream 15 km of river are shown in Figure 41 and Figure 42 below.

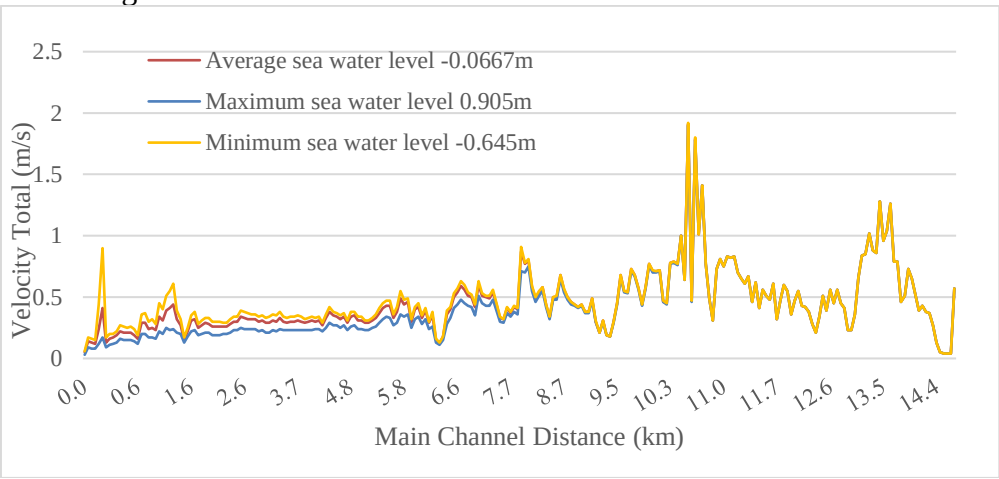

Figure 41. Comparison of velocities in the channel when the downstream sea water level at maximum, average and minimum for downstream 15km.

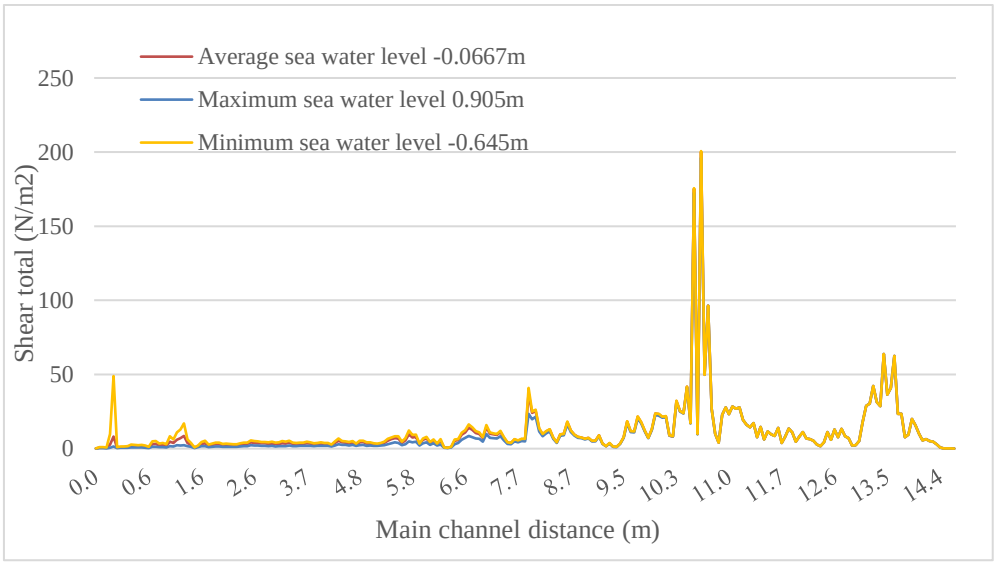

Figure 42. Comparison of shear stress when the downstream sea water level is at maximum, average and minimum for downstream 15km

Figure 41 and Figure 42 show that the worst-case scenario could influence about 10 km from the outlet of river, which is shown in the figure where sea water level has less effect on velocity and shear stress farther from the river outlet. Hence, the back-water flow effects from the sea water level on the flow of the river is clearly shown downstream. When the sea water level is at minimum both velocity and shear stress have higher values than when sea water level is at average and maximum. Moreover, when the sea water level is at maximum the river experiences higher back-water effects and produces lower shear stresses and velocities.

6.4 Sediment transport simulation results

6.4.1 Annual sediment transport along Viskan

Annual net sediment transport is the amount of sediment that leaves during the research periods. Since the equilibrium was selected as upstream boundary for sediment at cross section 110802 in catchment 2383, the HEC-RAS software brings in sediment from upstream to catchment 2383 and allows no change to occur to the first cross section which is same for the following catchment analysis. In order for better understanding Figure 43 shows the sub catchment

of Viskan with assigned cross sections. The sediment that entered catchment 2383 and the one that was calculated for the last cross section in the same catchment at cross section 89249 are presented in Figure 44 and Figure 45 below. Table 8 shows the difference of the sediment that enters and the one that leaves is calculated and results presented in it. In additional, all annual net sediment transport amounts shown below are not reliable values, there may be fluctuations of approximately 20 tonnes/year.

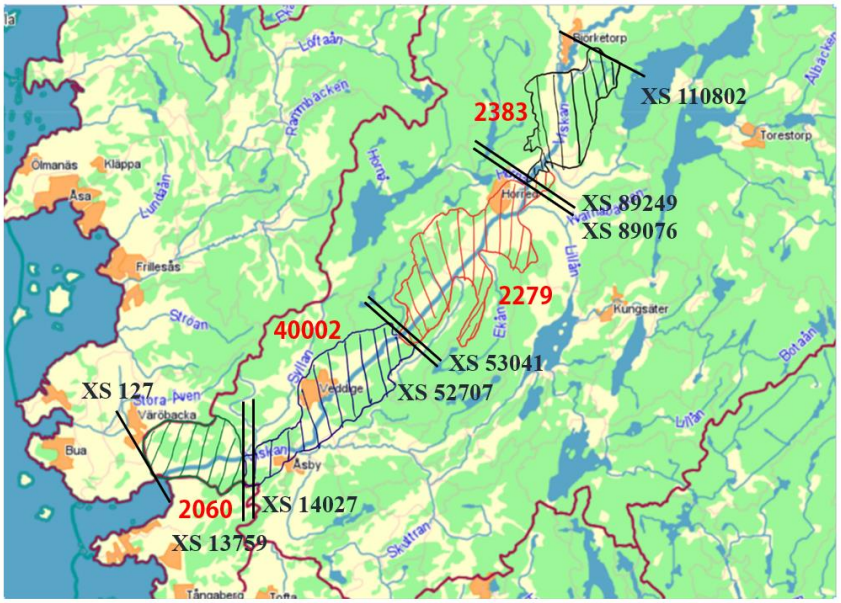

Figure 43. The sub catchment of Viskan with assigned cross sections

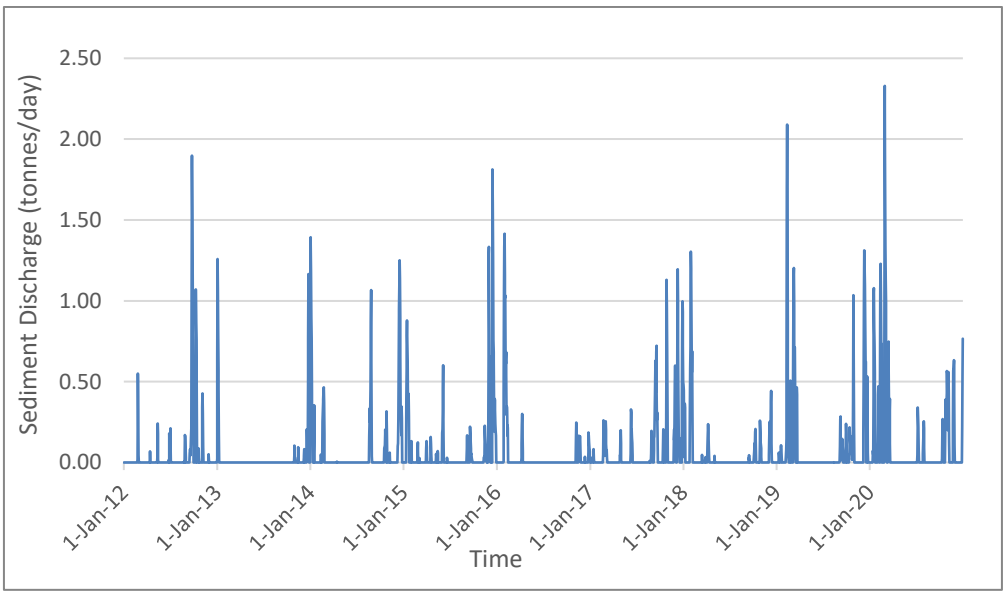

Figure 44. Sediment mass entering catchment catchment 2383 at the upstream cross-section 110802

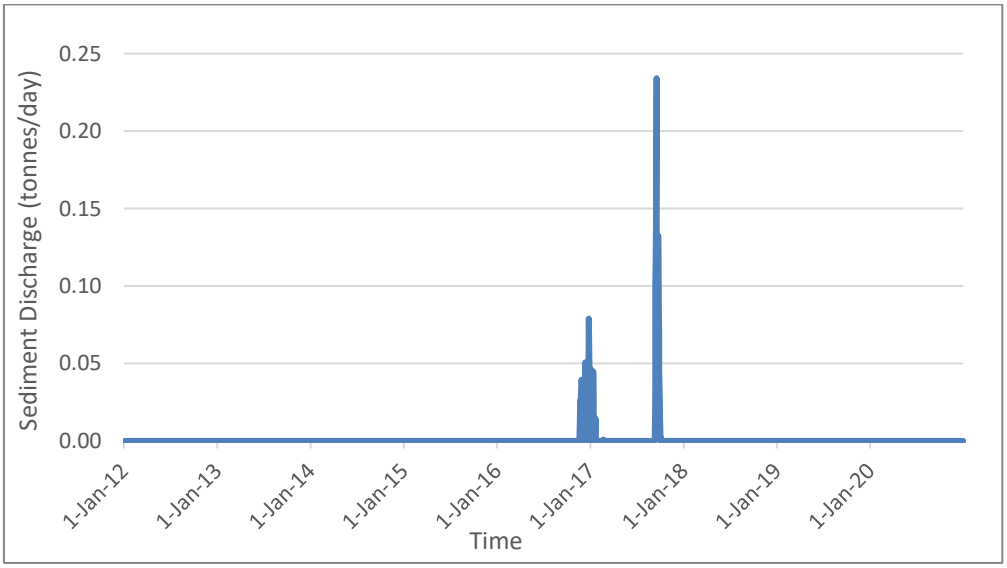

Figure 45. Sediment mass leaving catchment catchment 2383 at its last cross-section 89249

Table 8. Sediment transport per year for the upstream and downstream cross-section

	Sediment transport in Catchment 2383 (tonnes)		
Year	Upstream XS 110802	Downstream XS 89249	Net transport
2012	18	0	-18
2013	9	0	-9
2014	27	0	-27
2015	29	0	-29
2016	15	1	-14
2017	27	2	-25
2018	16	0	-16
2019	35	0	-35
2020	42	0	-42

The values that net transport that are positive represent erosion and for the one are negative represent deposition. The average deposition rate was 24 tonnes/year in catchment 2383. Further, sediment entering the catchment 2279 at cross section 89076 and leaving it at cross section 53041 was obtained and results are presented in Figure 46 and Figure 47 below. The difference between sediment mass at the first cross section 89076 and last cross section 53041 is presented in Table 9 below.

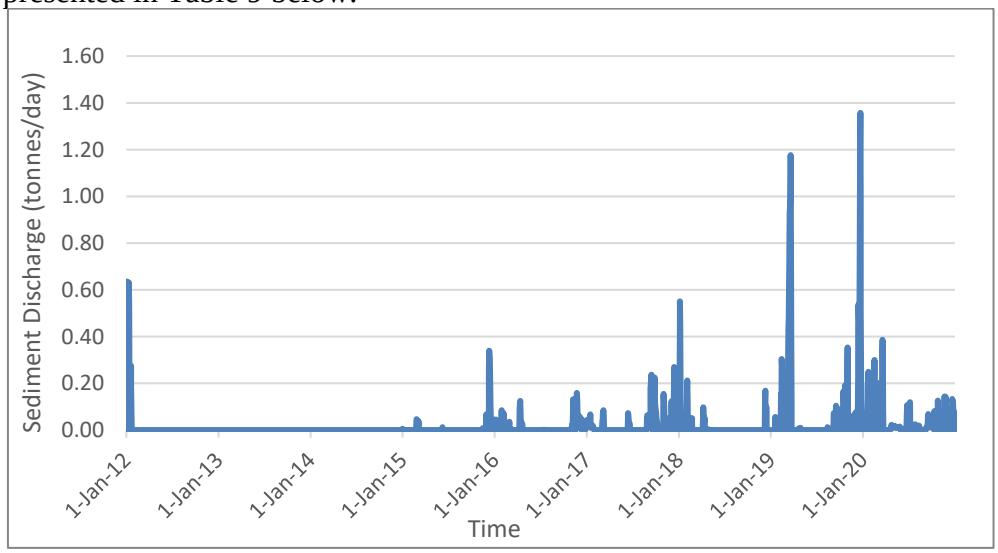

Figure 46. Sediment mass entering catchment 2279 at cross-section 89076

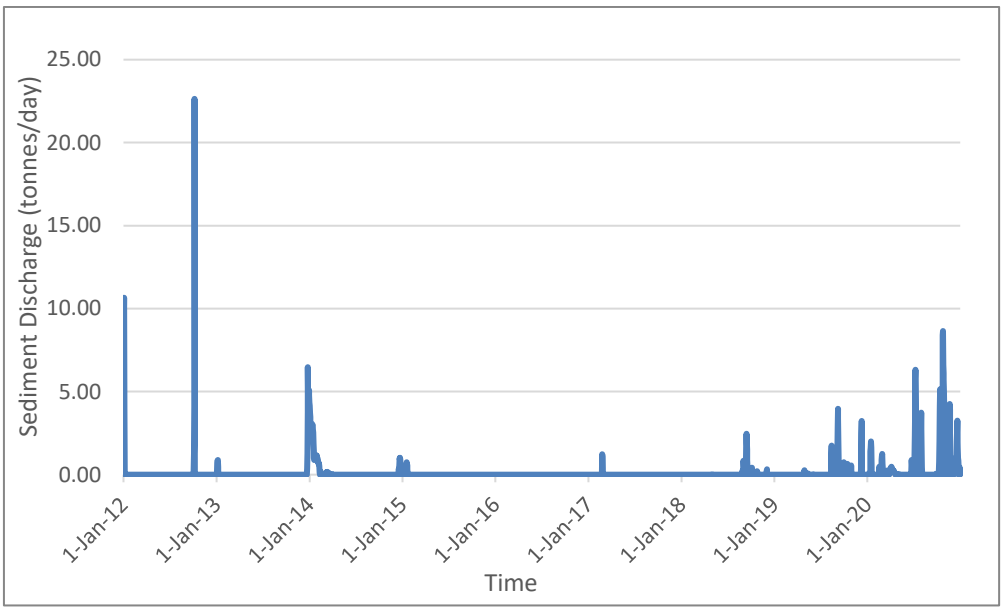

Figure 47. Sediment mass leaving catchment 2279 at cross-section 53041

Table 9. Sediment transport per year in catchment 2279

	Sediment transport in Catchment 2279 (tonnes)		
Year	Upstream XS 89076	Downstream XS 53041	Net transport
2012	5	53	48
2013	0	43	43
2014	0	74	74
2015	2	3	1
2016	4	0	-4
2017	7	3	-4
2018	4	15	11
2019	24	33	9
2020	10	174	165

The average erosion rate was 38 tonnes/year in catchment 2279. Sediment entering the catchment 40002 at cross section 52707 and leaving it at cross section 14027 was obtained and results are presented in Figure 48 and Figure 49 below. The sediment mass is presented in Table 10 below.

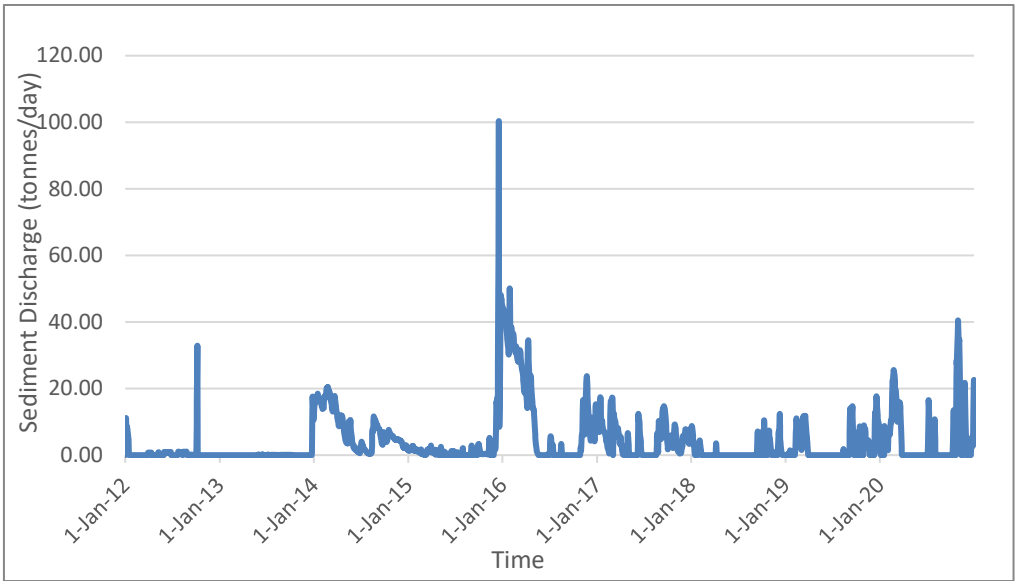

Figure 48. Sediment mass entering catchment catchment 40002 at cross-section 52707

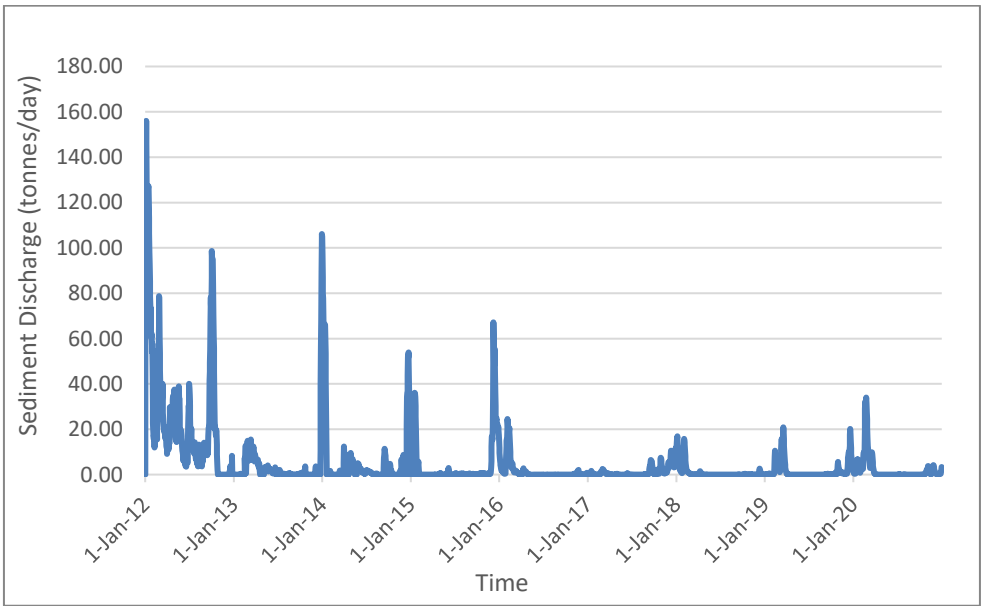

Figure 49. Sediment mass leaving catchment 40002 at cross-section 14027

Table 10. Sediment transport per year in catchment 40002

	Sediment transport in Catchment 40002 (tonnes)		
Year	Upstream XS 52707	Downstream XS 14027	Net transport
2012	241	8936	8695
2013	98	1256	1158
2014	2853	2067	-787
2015	1098	1342	245
2016	4416	509	-3907
2017	1686	451	-1234
2018	371	342	-29
2019	984	675	-309
2020	1814	765	-1049

The average erosion rate was 309 tonnes/year in catchment 40002. Then, sediment entering the last catchment 2060 at cross section 13759 and leaving it at the last cross section 127 is shown in Figure 50 and Figure 51 below. The sediment mass transport is shown in Table 11.

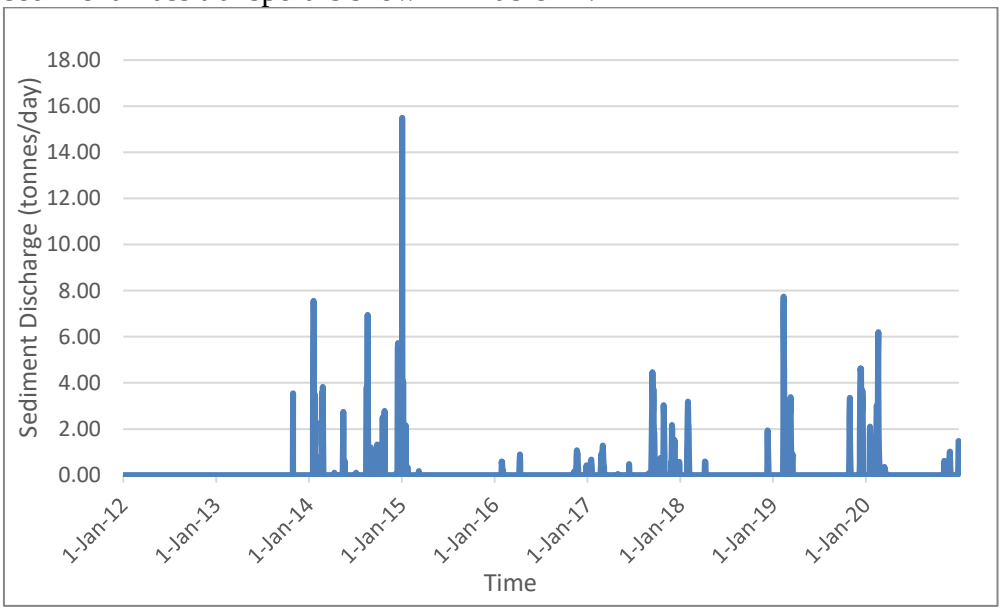

Figure 50. Sediment mass entering catchment catchment 2060 at cross-section 13759

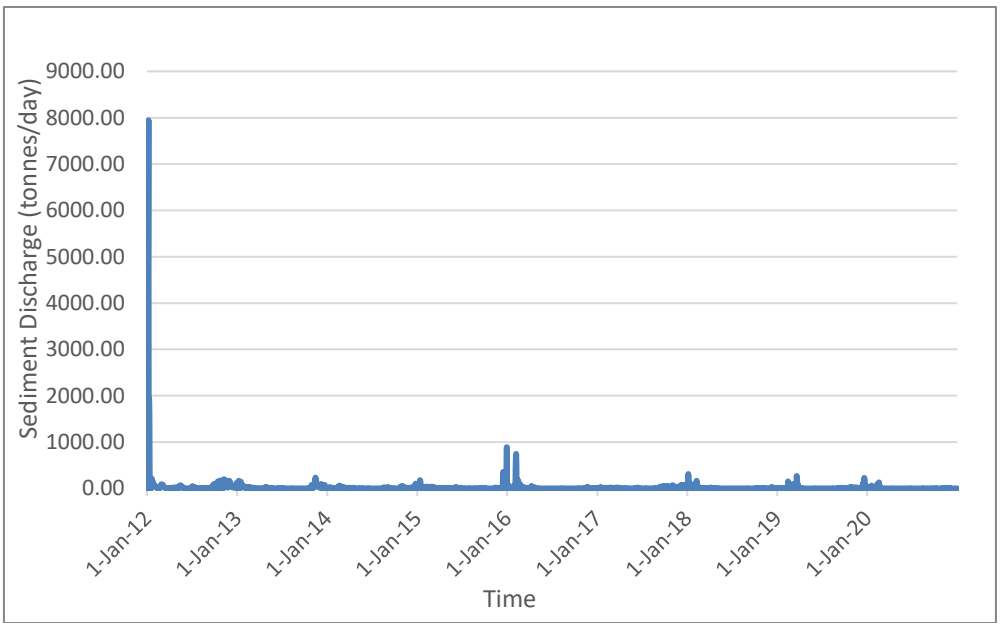

Figure 51. Sediment mass leaving catchment catchment 2060 at its last cross-section 127

Table 11. Sediment transport per year in catchment 2060

	Sediment transport in Catchment 2060 (tonnes)		
Year	Upstream XS 13759	Downstream XS 127	Net transport
2012	0	37653	37653
2013	4	6088	6084
2014	127	2666	2540
2015	26	4640	4614
2016	12	5667	5656
2017	76	3358	3282
2018	25	2549	2524
2019	110	3902	3793
2020	54	1182	1128

From Table 11 above, the averge yearly erosion that occurred in catchment 2060 was 7475 tonnes/year.

For better representation and analysis of sediment discharged at the last cross section 127, how the annual sediment mass transport differs from year to year is shown in Figure 52.

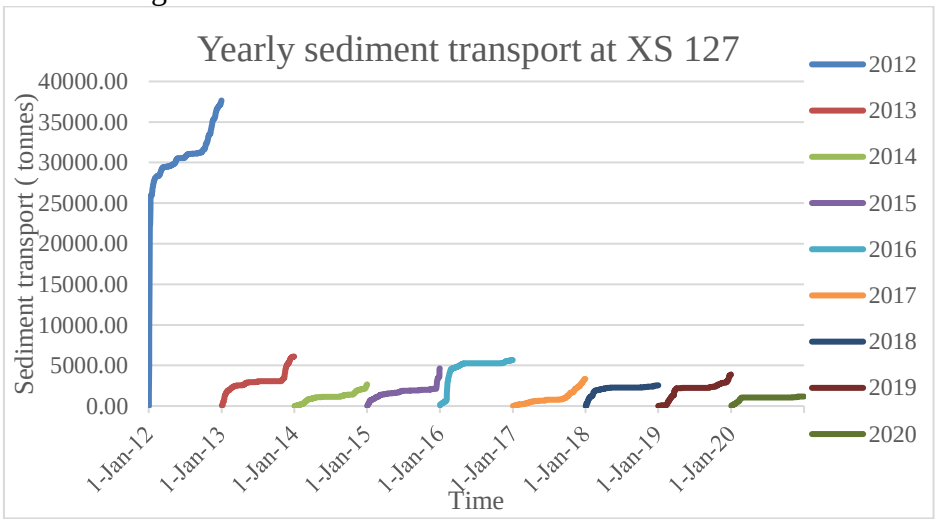

Figure 52. Cumulative Sediment discharge per year at the last cross-section 127 in catchment 2060

From the results for annual sediment discharge vary from year to year shown as Figure 52. The observed value for each year is listed in Table 12 with the annual average flow and their maximum flow.

Table 12. Annual sediment transport with annual average flow and maximum flow

Year	Sediment transport (tonnes/year)	Annual average flow (m^3/s)	Maximum flow (m^3/s)
2012	37635	51.7	183.0
2013	6078	30.9	193.0
2014	2639	44.5	161
2015	4611	47.3	223.0
2016	5653	31.6	153.0
2017	3331	44.4	143.0
2018	2533	31.8	156
2019	3867	45.7	183.0
2020	1140	48.8	210.0

From Figure 52 and Table 12, it is observed that year 2012 with the highest annual average flow had the highest sediment transport 37635 tonnes/year.

In order to determine in which year was net erosion and deposition, the calculation between the most upstream cross section 110802 and the most downstream cross section 127 is shown in Figure 53 below.

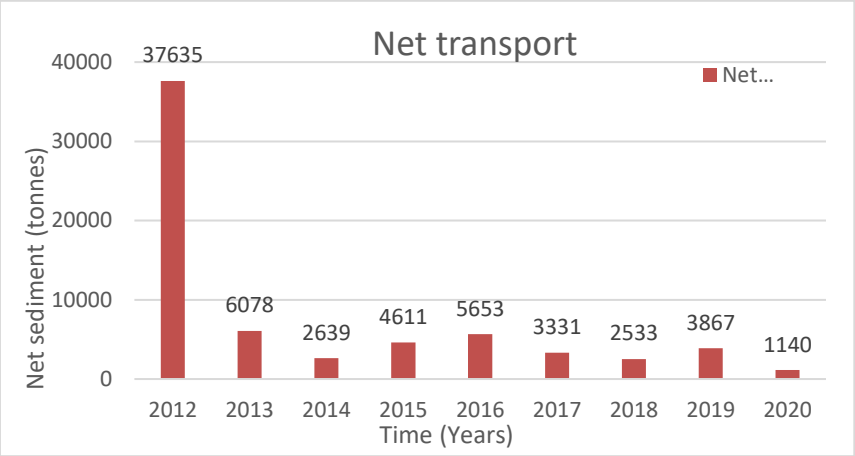

Figure 53. Net annual sediment budget for the Viskan study section

The results in Figure 53 show that all these 9 years had net erosion. Year 2012 shows the highest erosion 37635 tonnes. Followed by 2013 with 6078 tonnes and 2016 with 5653 tonnes. The reason of the highest erosion in 2012 is the average flow is the highest flow compared with other years shown as Table 12 and this year have high flows that occurred more frequently than others. Moreover, 2012 is the first modelling year the river cross sections were being more out of equilibrium with the flow compared to the subsequent years which could also cause higher transport.

6.4.2 Bathymetry changes as a result of sediment transport simulation

After simulation, the changes in bathymetry that occurred at each cross section were noted. The Figure 54 to Figure 56 showcase a few of cross sections that had erosion and some that had deposition and others with no change.

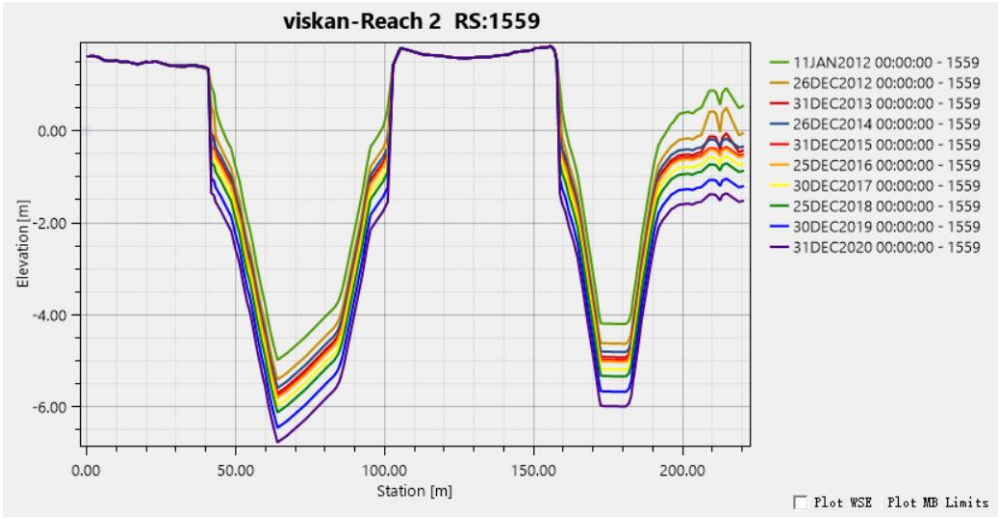

Figure 54. Cross section showing erosion

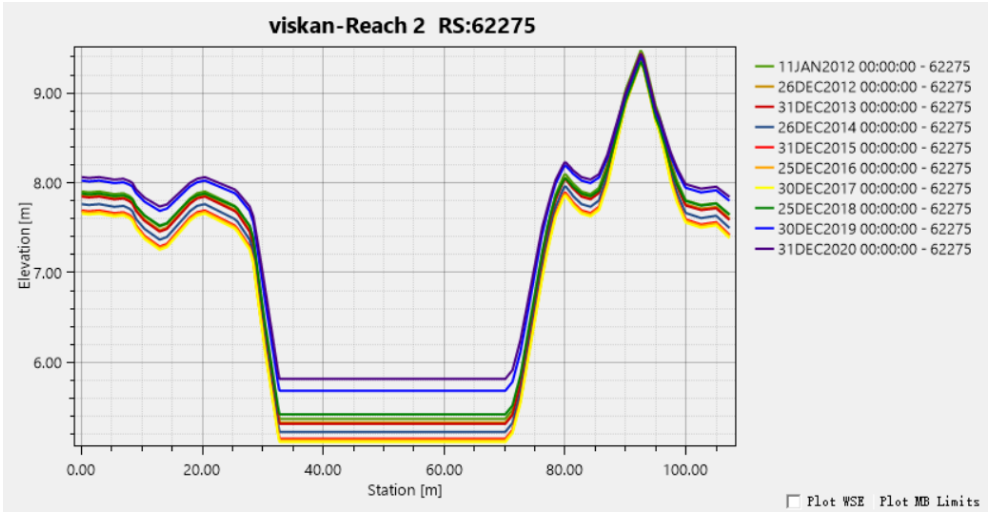

Figure 55. Cross section showing deposition

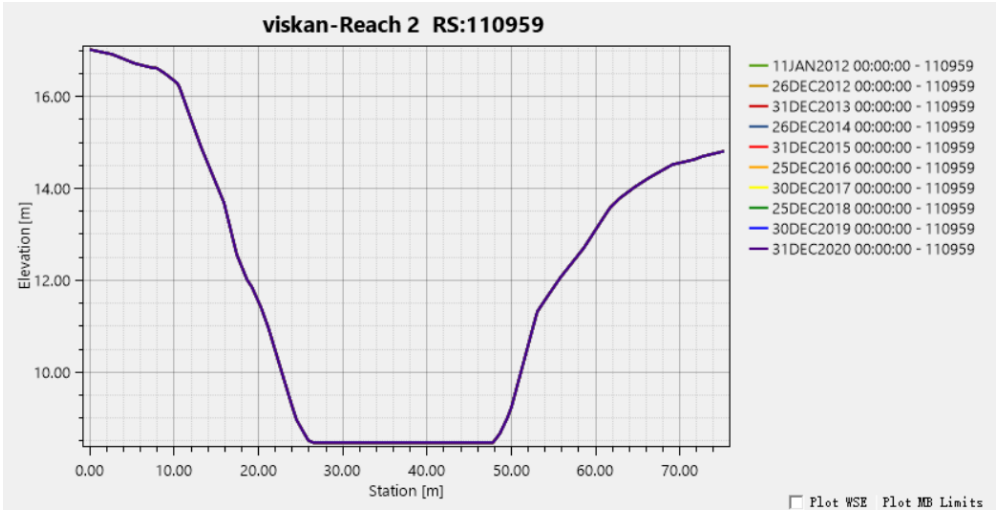

Figure 56. Cross section showing no change

6.4.3 Local scour mapping and geometric analysis

Through HEC-RAS a model of sediment transport in Viskan has been developed. It was also possible to find several bed anomalies along the studied 33.78 km river. In this report, only the most extreme conditions of holes will be focused which is shown in the Figure 57 below. The cross sections that eroded and had depositions were selected and are presented in appendix 2.

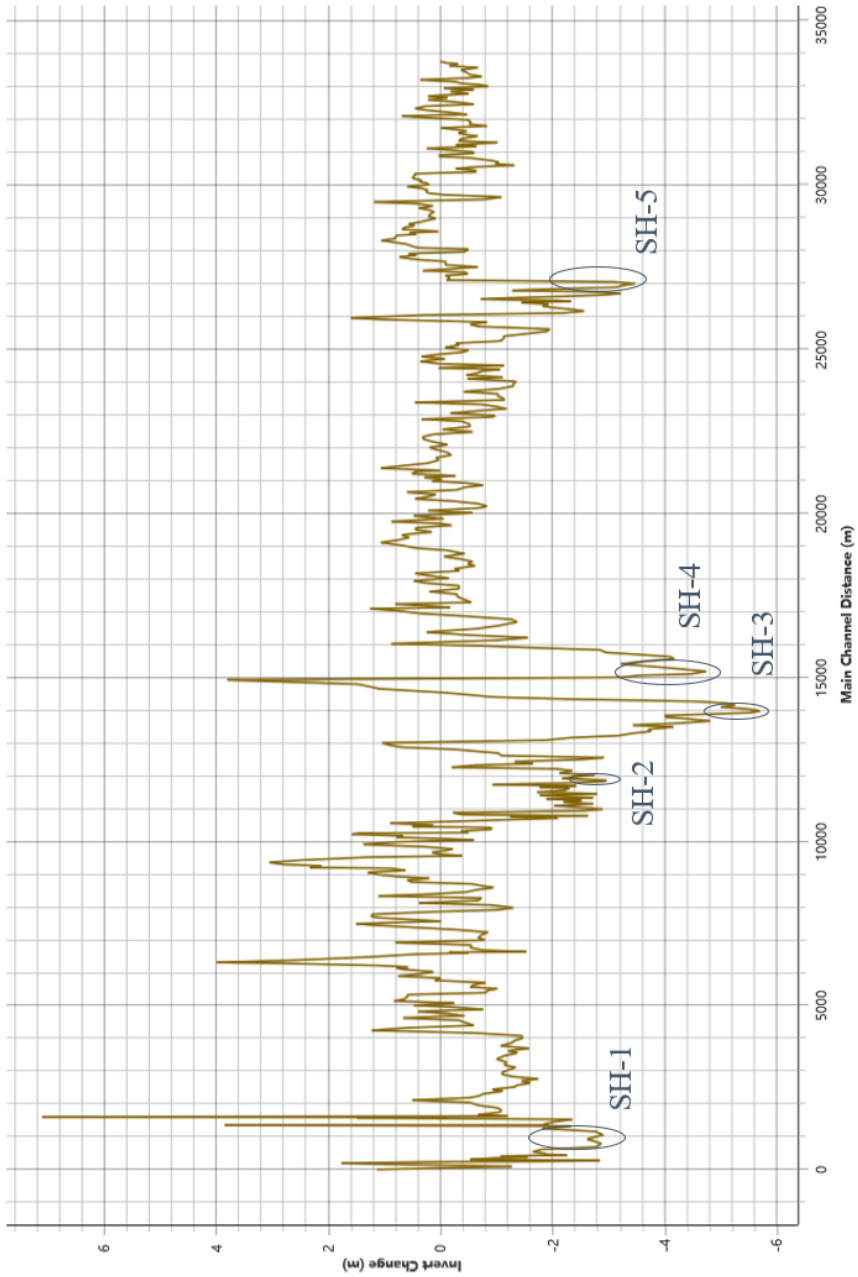

Figure 57. The longitudinal river bed profile with possible scour holes along Viskan

Obstacles in river like bridges cause flow separation can lead to scour holes and deposition (Euler and Herget, 2010). The holes were characterized by the presumed controlling mechanism as bend scour, bridge scour, and general scour from changes in bed conditions (Inamdeen, 2019). The possible causes of the scour holes and are presented in Table 13.

Table 13. Possible causes of the identified scour holes

Hoel ID	Location	Possible causes
SH-1	686.2 m	The scour hole is located in front of the river delta. High probability for hard bottom scouring and caused deposition behind as delta.
SH-2	11825.4 m	The scour hole is located on the bend where had a series erosion. Because there are many consecutive bends at this location which cause high probability for bend scouring. The bend influenced flow velocity and shear stress be higher.
SH-3	13979.9 m	The scour hole is located downstream of a narrow river cross section. The narrow section at upstream of the hole is resistant for average flows and the water velocity is increased which might be the reason of holes.
SH-4	15186 m	The scour hole is located near a marshy land which is no structures close to hole and no bend. Therefore, the formation of this scour hole may be influenced by the presence of hard bottom downstream.
SH-5	27005.6 m	This scour hole is same as SH-3 which is located no close to structures and no bend. Thus, there may be a hard bottom downstream of the scour hole which causes the scour hole.

6.4.4 Results of observed erosion in HEC-RAS

In order to have a better version of the actual situation of the Viskn river, on 5th May 2022, with the assistance of SGI a field trip along Viskn was carried out. Through the field trip of Viskan five places erosion were observed. By

simulating the sediment transport of HEC-RAS, the corresponding cross section is compared with the pictures. The cross sections correspond are XS 5288, XS 22041, XS 34314, XS 85790 and XS 86883. Figure 58 shows the cross sections from HEC-RAS and their corresponding pictures.

Cross sections from HEC-RAS	Pictures corresponding to cross sections
XS 5288 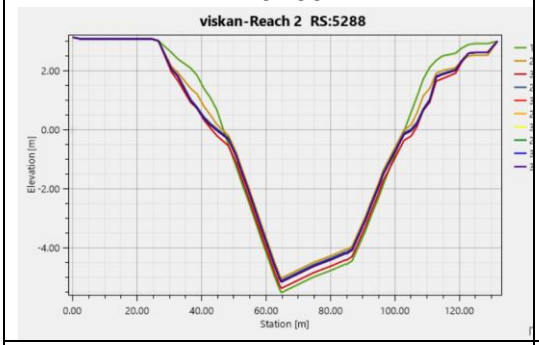	
XS 22041 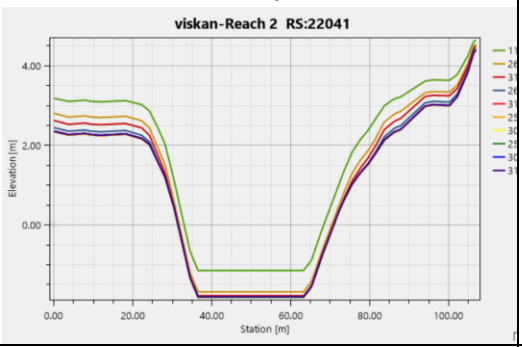	
XS 34314 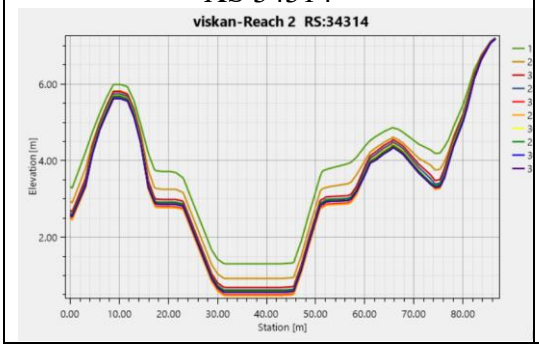	

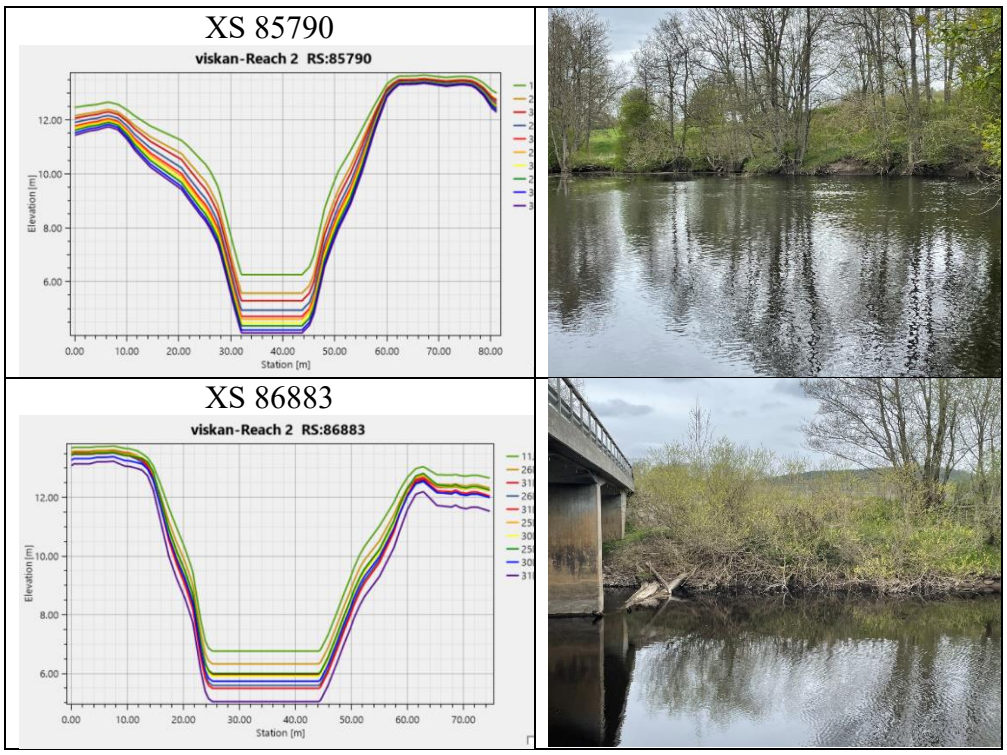

Figure 58. Erosive cross sections and corresponding pictures

Cross section 22041, 34314, 85790 and 86883 all show heavy erosion from HEC-RAS which is confirmed by the pictures from field visit.

However, cross section 5288 shows no erosion at river bed from HEC-RAS but with bank failure. Through the pictures there is bank erosion. Moreover, through the introduction by surrounding residents, this field had erosion before but they have filled the area with protective material by themselves. Therefore, the reason of no erosion show from HEC-RAS may be the filling material is hard which cause less erosion for river bed but the bank erosion is still can be seen from both HEC-RAS results and picture.

6.4.5 Comparison of different transport functions

In order to compare how different functions influence the HEC-RAS sediment transport model, Figure 59 have shown the longitudinal river bed profile along Viskan using different sediment transport functions. These results are all the invert change along Viskan for the period 2020. The separate longitudinal river

bed profiles along Viskan using the different functions are shown in appendix 3.

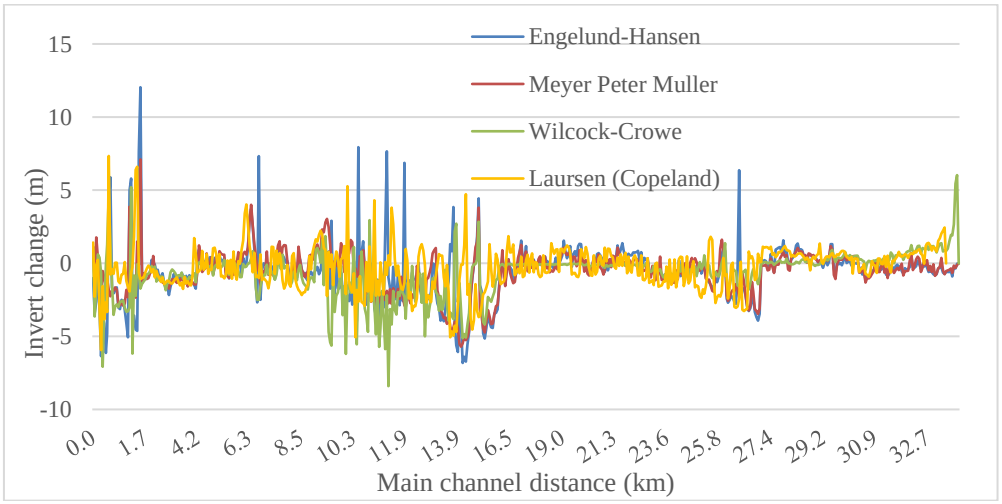

Figure 59. The longitudinal river bed profile along Viskan with different functions

Through Figure 59 the Laursen (Copeland) transport function is the most sensitive one which shows more changes at the same locations. The Wilcock-Crowe transport function is least sensitive to bathymetry changes which shows the gentlest changes at upstream part but this transport functions shows the deepest erosion compared with others.

The Engelund-Hansen transport functions are more sensitive for deposition which shows the most depositions along Viskan. Most sediment transport functions are based either on shear stress or stream power. They usually use an excess-shear or excess-power form, which compares the actual shear or power to a threshold. HEC-RAS does not compute any transport for that grain class if it is below the threshold. The Engelund-Hansen transport function is not an excess form of the stream power equation, but just a function of stream power using the product of velocity and shear stress (τV) (Gibson and Sánchez, 2020). This might be the reason why the Engelund-Hansen transport function is more sensitive to sediment accumulation because the way this function compares with the threshold is different.

The Meyer-Peter and Müller transport function is the most balanced function which has the gentlest change compared with other functions. This transport

function is one of the earliest equations developed. It is a simple excess shear relationship. The Meyer-Peter and Müller transport function is most applicable in gravel systems and tends to under-predict transport of finer material (US Army Corps of Engineers, 2020). Therefore, the grain size will influence the output. This might be the reason for the insensitivity of the Meyer-Peter and Müller transport function.

7 Discussion and Conclusion

7.1 Discussion

The HEC-RAS hydrodynamic simulation for the average flow reveal the water surface profile, show as Figure 38, at the location of hydropower station has a big elevation drop. Moreover, the water velocity and shear stress are very high at locations do not cause scour hole where is also influenced by the hydropower station. The scour holes are all around the bends, the river narrows and bridges. From Figure 39, the highest velocities obtained were 1.91 m/s at 10.5 km and 0.87m/s at 7.85 km around downstream. As for the minimum velocity was 0.04 m/s at 14.92 km where had deep scour holes. For these locations from Figure 40 the shear stress was 200.10 N/m^2 at 10.5 km, 37.18 N/m^2 at 7.85 km and 0.04 N/m^2 at 14.92 km. In Figure 41 and Figure 42 shows the downstream sea water level has a great impact on the hydraulic parameters in the river. When the sea water level is at minimum there is no back-water flow effect where the velocity at 7.85 km close to downstream is 0.91 m/s with the shear stress 41.05 N/m^2 compared with the average sea water level the velocity and shear stress all become higher.

The results for sediment transport simulation revealed that the upstream catchment 2383 is dominated by deposition at the rate of 24 tonnes/year, for the catchment 2279 with the erosion rate of 38 tonnes/year, catchment 40002 with the erosion rate of 309 tonnes/year and the most downstream catchemnt 2060 at the erosion rate of 7475 tonnes/year. From Table 12 and Figure 52, it is observed year 2012 with the highest annual average flow had the highest sediment transport at catchemnt 2060 up to 37635 tonnes/year. Furthermore, from 2012 to 2020 the river shows a net annual erosion.

After sediment transport simulations, 5 most eroded cross sections XS 2374, XS 38919, XS 45988, XS 49945 and XS 88725 are used for possible causes analysis. XS 2374, XS 49945 and XS 88725 are the hard bottom scour erosion. Moreover, XS 38919 is bend scour and XS 45988 is due to the river become narrow at upstream. Then the observed erosion compared with simulation results was taken at XS 5288, XS 22041, XS 34314, XS 85790 and XS 86883 and all the cross sections are shown reasonable results from HEC-RAS.

Furthermore, in order to comparison of different transport functions the Meyer-Peter and Müller transport function, the Laursen (Copeland) transport function,

the Engelund-Hansen transport functions and the Wilcock-Crowe transport function were used for simulations. The Laursen (Copeland) transport function is the most sensitive one, the Wilcock-Crowe transport function is least sensitive to bathymetry changes. The Engelund-Hansen transport functions are more sensitive for deposition and the Meyer-Peter and Müller transport function is the most balanced function with the gentlest changes.

7.2 Conclusion

The focus of the report was to estimate the transport of sediment along Viskan and extend this to find possible erosion locations. The scope extended to comparison the different transport functions.

The first step to achieve results for this study was to setup the model and the Digital Elevation Model was needed for this study. After finished the HEC-RAS Mapper where the river reach, bank lines and flow path and cross sections were drawn. Before simulation the calibration of applicable Manning's n values for the left, right and main channel was assigned. After being satisfied with the attained Manning's n values the steady flow simulation was done to understand hydraulic parameters within the river and the effect of downstream sea water level. This analysis revealed that when the sea water level is at its minimum, the velocities and shear stress close to the downstream are going high due to less back-water flow effect from the sea. Further sediment transport simulation was done with quasi-unsteady flow and the period of the flow considered was from 2012 to 2020.

The sediment transport simulation revealed that there was deposition occurring in catchment 2383 at a rate of 24 tonnes/year, erosion occurred at catchment 2279 with the rate of 38 tonnes/year, erosion at the rate of 309 tonnes/year at catchment 40002 and the most downstream catchment 2060 with the erosion rate of 7475 tonnes/year. Furthermore, five cross sections were found to be the most erosive cross sections and four observed locations were compared with the results of simulation. Lastly, the comparison of different sediment transport functions was researched.

8 Limitations and Recommendations

8.1 Limitations

During the carrying out of this study, several limitations existed that could affect results and the biggest of them being the lack of the sediment gradation data. For this study, there is no specific sediment gradation therefore only can refer and estimate a reasonable value. And there were no sediment discharge observations to use to generate a sediment rating curve and be used for calibration and validation of the sediment transport simulation. Additionally, this study assumed there is no sediment load from other joining stream which do not match reality. The Digital Elevation Model is lack of upstream data and the data of the hydropower station, caused the results of the upstream and around hydropower station was sketchy. Also, the calibration data was insufficient and the dates of the data was unclear the study can only assume the date which could make the calibration inadequate and inaccurate. Moreover, the calibration is only one day data which is not enough for calibration and could cause the results uncertain. Finally, the effect of climate change on sediment was not be considered during this study.

8.2 Recommendations

As recommendations, more measurement of water surface level for calibration long Viskan could assist in attaining more accurate results. Also, the study of the sediment gradation would be helpful for the research of the sediment transport. Having equipment installed to measure sediment discharge in Viskan and other Swedish rivers would be useful in generating a sediment rating curve applied at the upstream cross section as a boundary condition and also assist in calibration and validation of sediment discharge. Lastly, more accurate Digital Elevation Model data along river would make the research of sediment and flow more precise.

References

Blyth, F. G. H., & De Freitas, M. (2017). A geology for engineers (7th Ed). CRC Press.

Brandt, M. (2017). Generation, Transport and Deposition of Suspended and Dissolved Material – Examples from Swedish Rivers.

Brunner, G. W. (2021). HEC-RAS River Analysis System: User's Manual, Version 6.0, US Army Corps of Engineers, Institute for Water Resources, Hydrologic Engineering Center.

Soulsby, R. (1997). Dynamics of marine sands: A manual for practical applications, Thomas Telford.

Camenen, B. & Larson, M. (2007). A Unified Sediment Transport Formulation for Coastal Inlet Application, US Army Corps of Engineers, Institute for Water Resources, Hydrologic Engineering Center.

Engdahl, M & Pile, O. (2019). Geologisk beskrivning av Viskans och Häggåns dalgångar.

Engelund, F & Hansen, E. (1967). A monograph on sediment transport in alluvial
streams. Copenhagen: Teknisk Forlag.

Euler, T & Herget, J. (2010). Controls on local scour and deposition induced by obstacles in fluvial environments. [online] Available at: https://doi.org/10.1016/j.catena.2010.11.002

Flynn, R. H. (2011). Analysis of the transport of sediment by the Suncook River in Epsom, Pembroke, and Allenstown, New Hampshire, after the May 2006 flood. US Department of the Interior, US Geological Survey.

Gibson, S & Sánchez, A (2020). HEC-RAS Sediment Transport: User's Manual, Version 6.0, US Army Corps of Engineers, Institute for Water Resources, Hydrologic Engineering Center.

Hoek, E., & Bray, JD (1981). Rock slope engineering (3rd Ed). CRC Press.

Inamdeen, F. (2019). Evaluation of Local Scour along Rönne Å at Ängelholm, Lund University.

Julien, P Y. (2018). River Mechanics 2nd edition, Cambridge University Press. [online] Available at: https://doi.org/10.1017/9781316107072

Modigh, A., Fredrikson, F., Wolme, S & Magnusson, J. (2012). Klimatanpassning Viskan.

Norström, E. (2021). Digitalisering av historiska jordartsprofiler från Viskans dalgång. [online] Available at: https://resource.sgu.se/dokument/publikation/sgurapport/sgurapport202126rapport/s2126-rapport.pdf

Partheniades, E. (2009). Cohesive sediments in open channels: erosion, transport and deposition. Butterworth-Heinemann.

Rai, R. & Singh, G., n.d. E-Content on Slope Engineering. [Online] Available at: http://www.iitbhu.ac.in/faculty/min/rajesh-rai/NMEICT-Slope/Pdf/03%20Types%20of%20slope%20failure.pdf

Rankka, W. (2022). Erosion utmed Viskan enligt MSB Skredriskkarteringar.

Rijn, L C. (1984). Sediment Transport, Part I: Bed Load Transport. [online] Available at: https://doi.org/10.1061/(ASCE)0733-9429(1984)110:10(1431)

SWECO. (2014). Avvägning av kontrollpunkter vid Vattenfallsdammar i Viskan 2014.

Vattenwebb.smhi.se. 2022. Vattenwebb - Modelldata Per Område. [online] Available at: https://vattenwebb.smhi.se/modelarea/.

Yang, CT (2006). Erosion and sedimentation manual. US Dep. of the Interior, Bureau of Reclamation, Denver, CO.

Appendices

Appendix 1:

A zoom in view of constructed cross sections in parts of Viskan for model analysis

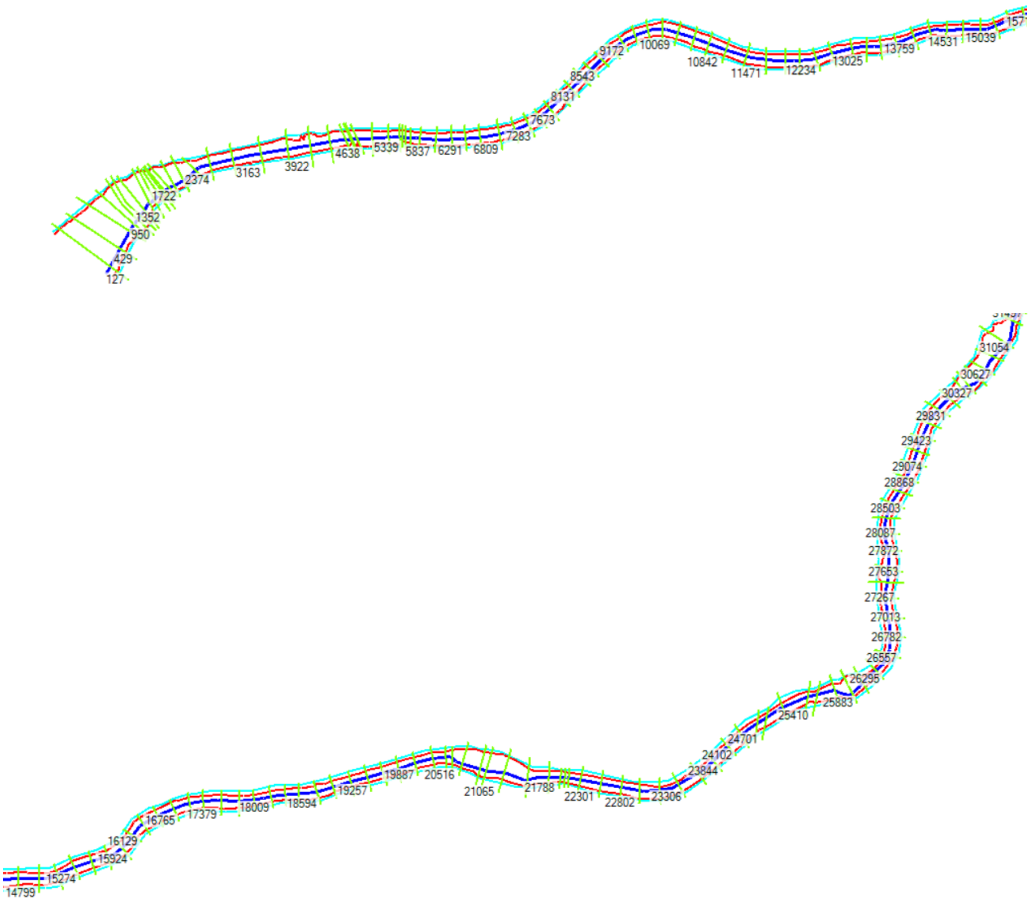

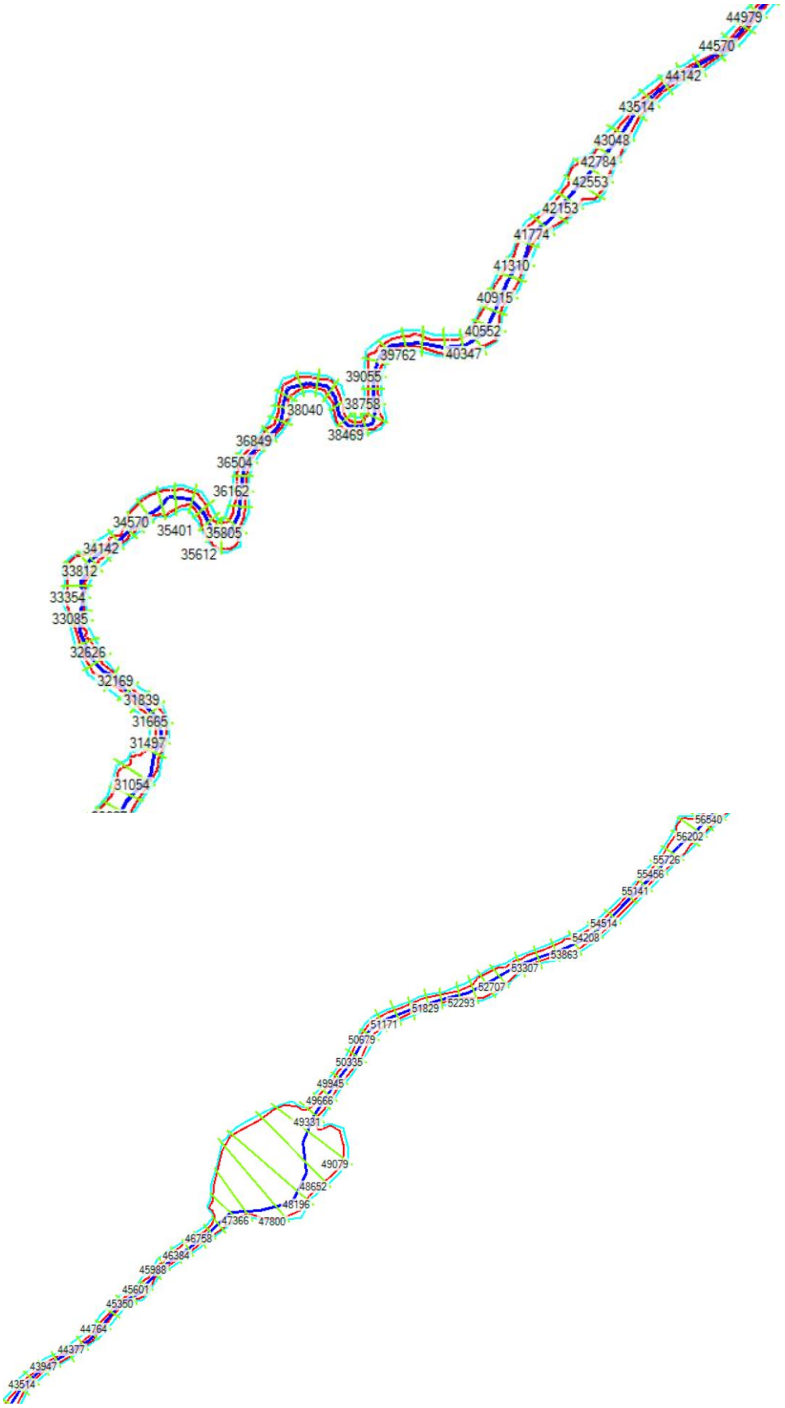
44979
44570
44142
43514
43048
42784
42553
42153
41774
41310
40915
40552
40347
39762
39055
38758
38469
38040
36849
36504
36162
35805
35612
35401
34570
34142
33812
33354
33085
32626
32169
31839
31665
31497
31054
56540
56202
55726
55456
55141
54514
54208
53863
53307
52707
52293
51829
51171
50679
50335
49945
49666
49331
49079
48652
48196
47800
47366
46758
46384
45988
45601
45350
44764
44377
43947
43514

Figure 1.1. Drawn cross sections along Viskan with RAS Mapper in HEC-RAS 6.1.0 showing 110959 as first cross section for upstream and 127 as last cross section for downstream.

Appendix 2:

Most eroded cross sections and deposition cross sections.

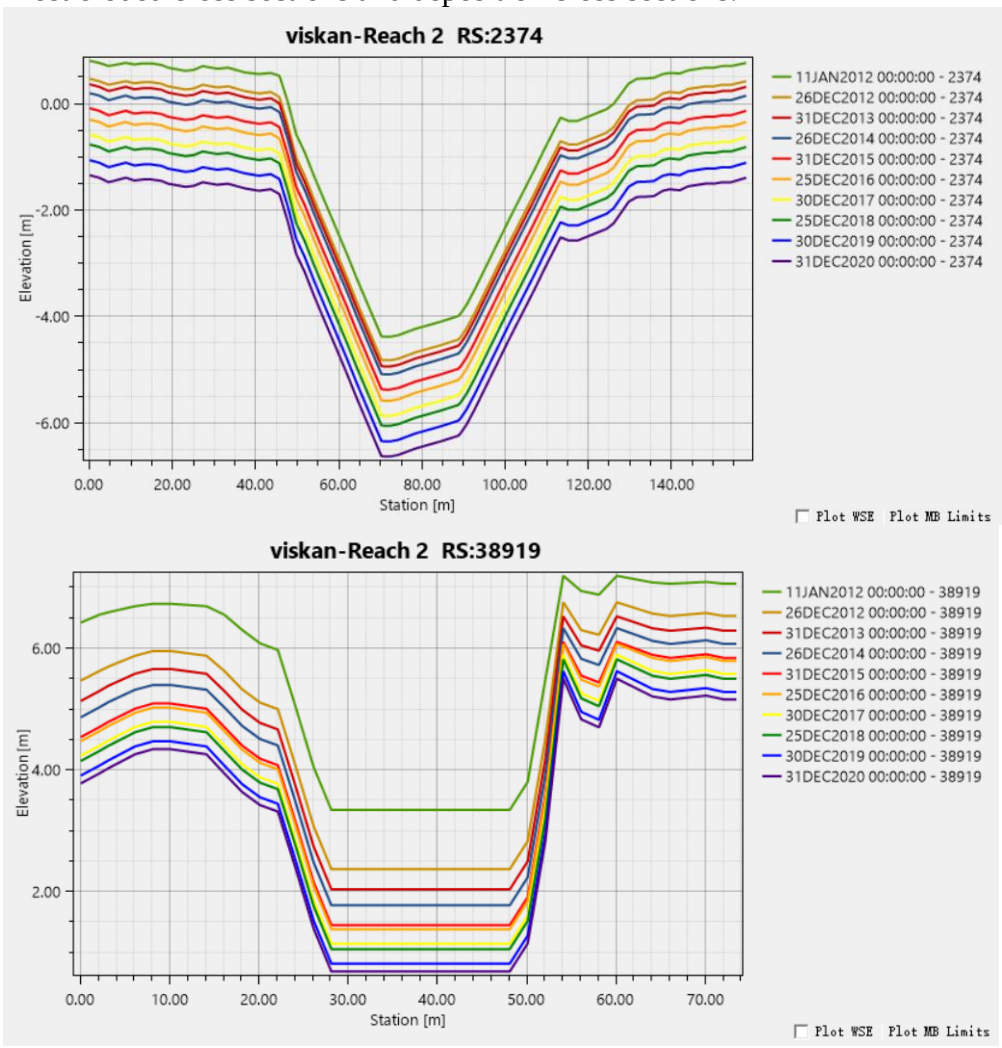

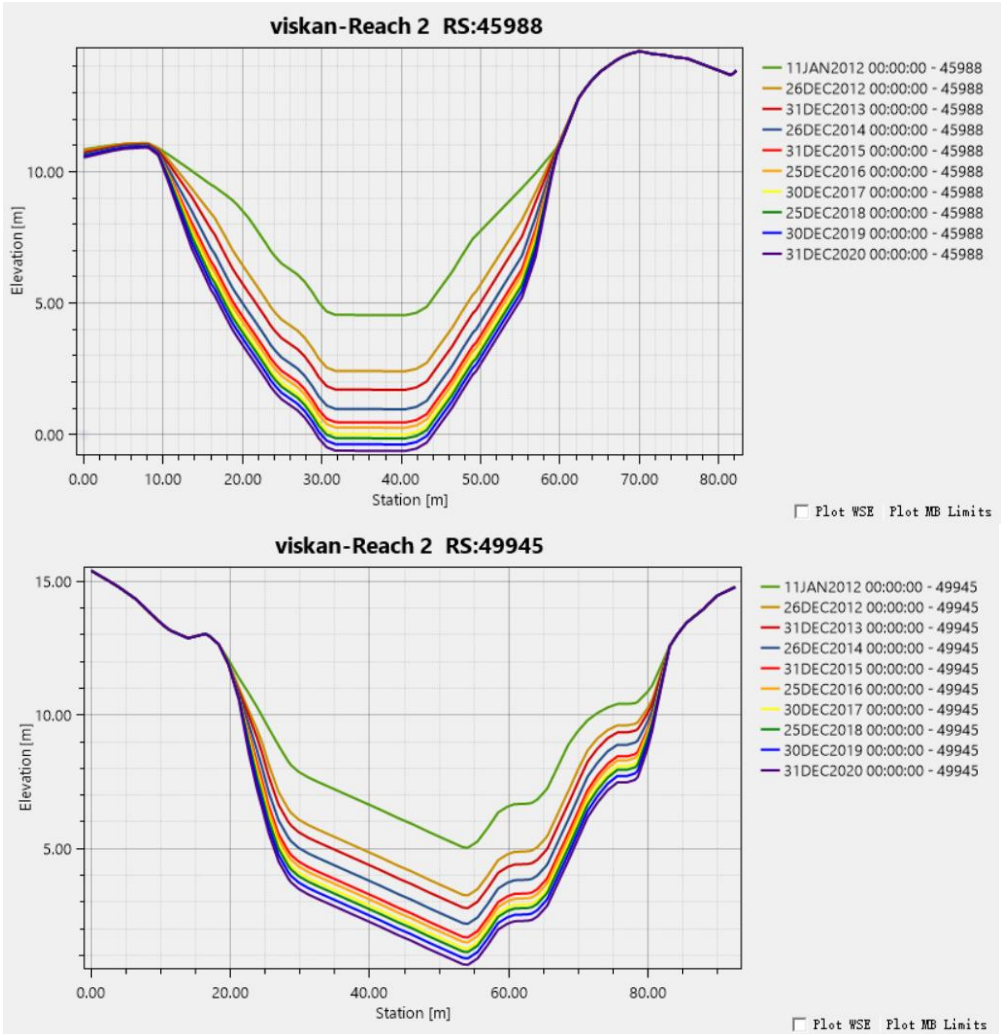
viskan-Reach 2 RS:45988
Elevation [m]
10.00
5.00
0.00
0.00
10.00
20.00
30.00
40.00
50.00
60.00
70.00
80.00
Station [m]
11JAN2012 00:00:00 - 45988
26DEC2012 00:00:00 - 45988
31DEC2013 00:00:00 - 45988
26DEC2014 00:00:00 - 45988
31DEC2015 00:00:00 - 45988
25DEC2016 00:00:00 - 45988
30DEC2017 00:00:00 - 45988
25DEC2018 00:00:00 - 45988
30DEC2019 00:00:00 - 45988
31DEC2020 00:00:00 - 45988
Plot WSE
Plot MB Limits
viskan-Reach 2 RS:49945
Elevation [m]
15.00
10.00
5.00
0.00
20.00
40.00
60.00
80.00
Station [m]
11JAN2012 00:00:00 - 49945
26DEC2012 00:00:00 - 49945
31DEC2013 00:00:00 - 49945
26DEC2014 00:00:00 - 49945
31DEC2015 00:00:00 - 49945
25DEC2016 00:00:00 - 49945
30DEC2017 00:00:00 - 49945
25DEC2018 00:00:00 - 49945
30DEC2019 00:00:00 - 49945
31DEC2020 00:00:00 - 49945
Plot WSE
Plot MB Limits

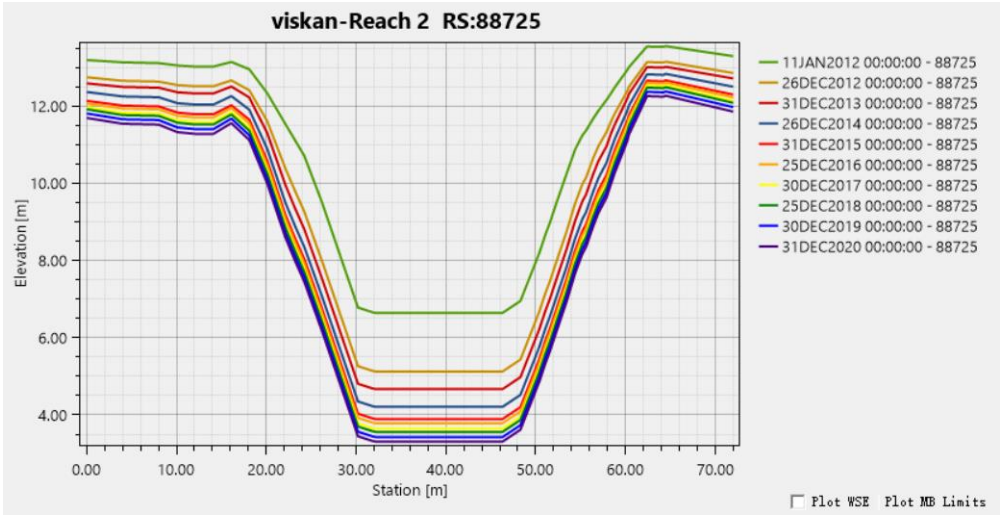

Figure 2.1. Erosive crosssections from sediment transport in HEC-RAS

Appendix 3:

The longitudinal river bed profile with different transport functions

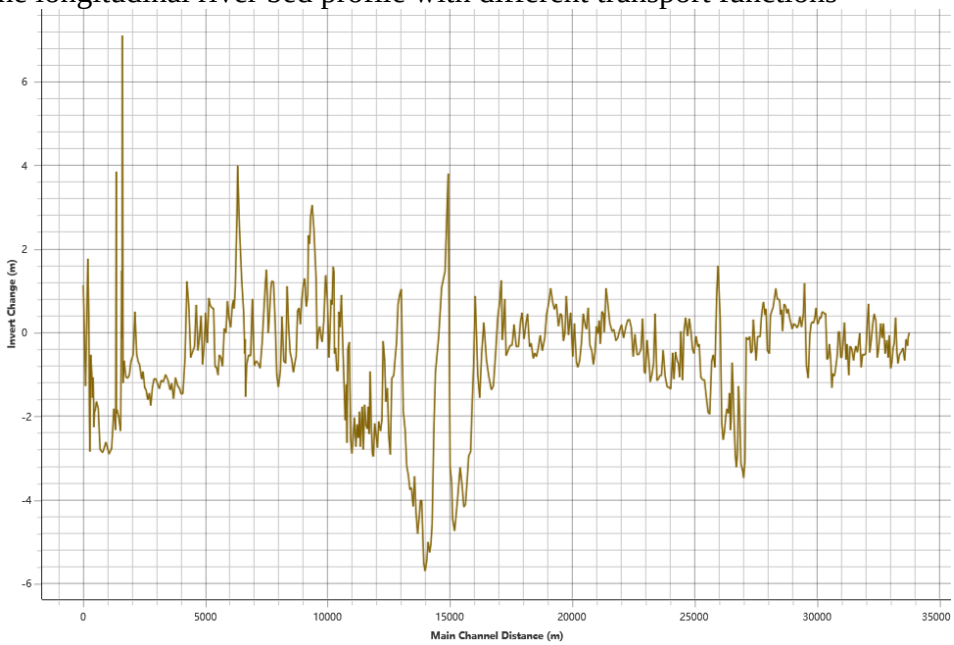

Meyer-Peter and Müller transport function

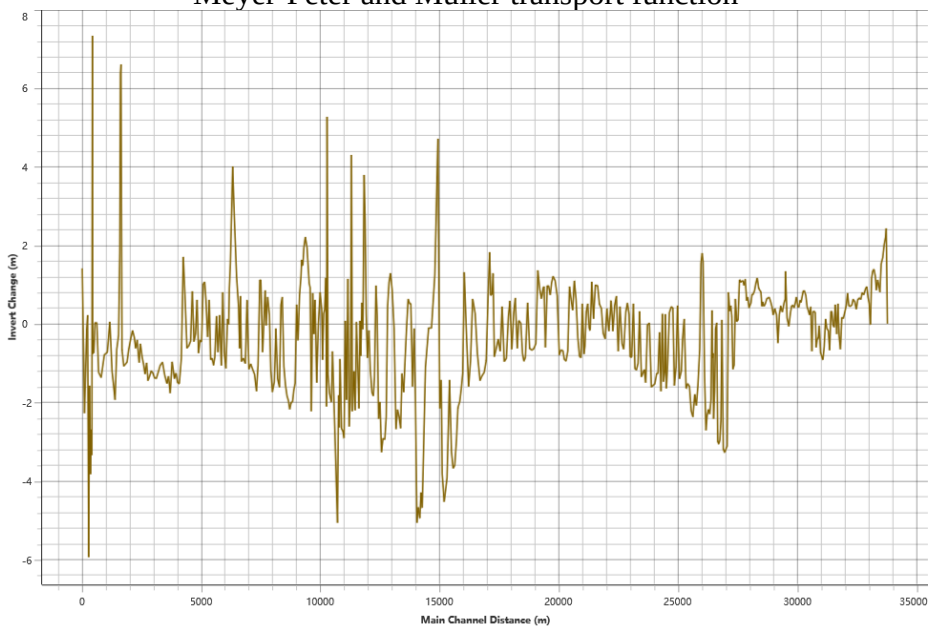

Laursen (Copeland) transport function

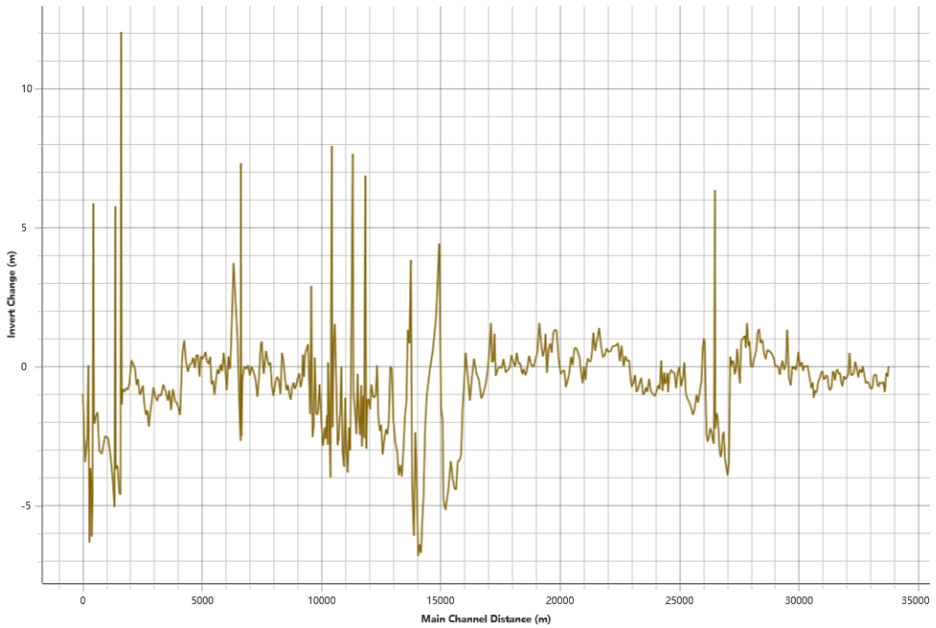

Engelund-Hansen transport function

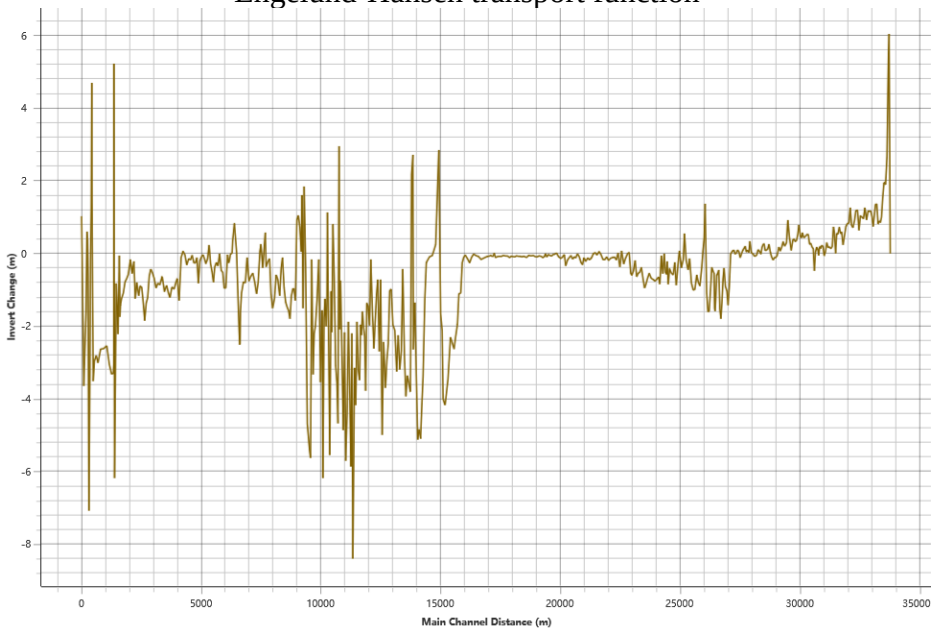

Wilcock-Crowe transport function

Figure 3.1. The longitudinal river bed profile along Viskan with different transport functions.